ABSTRACT

MEASUREMENT OF MICROCARRIER WEIGHTED FLOC USING THE ENVIRONMENTAL ELECTRON MICROSCOPE

by
Viriya Vithayaveroj

Utilizing the concept of coagulation in conjunction with the sediment enhancement by microcarrier, the microcarrier process has been demonstrated in a laboratory investigation as an effective and economic operation in removing colloidal particles in an aquatic system. The microcarrier, an inert aluminum silicate particulate (Ottawa Sand) of 53 to 75 micrometers in diameter was used in this study. The interaction between the flocs and the microcarriers plays an important role in the mixing process. The principal objective of this study is to examine the structural interaction between the flocs and the microcarrier.

The study was designed into two stages, the prescreening stage and the observation under the ESEM stage. In the first stage, a series of jar test using microcarrier along with electrolyte and polyelectrolyte were carried out in which the turbidity was the control parameter. On the second stage, the Environmental Scanning Electron Microscope (ESEM) was used to investigate the structural relationship between the microcarrier and flocs. The visual structural information was achieved under this microscope technique. A 99.6% of turbidity removal could be achieved by the microcarrier process.

MEASUREMENT OF MICROCARRIER WEIGHTED FLOC USING THE ENVIRONMENTAL ELECTRON MICROSCOPE

by
Viriya Vithayaveroj

A Master's Thesis
Submitted to the Faculty of
New Jersey Institute of Technology
In Partial Fulfillment of the Requirements for the Degree of
Master of Science in Environmental Engineering

Department of Civil and Environmental Engineering

January 2000

APPROVAL PAGE

MEASUREMENT OF MICROCARRIER WEIGHTED FLOC USING THE ENVIRONMENTAL ELECTRON MICROSCOPE

Viriya Vithayaveroj

Dr. Yuan Ding, Thesis advisor — Date
Assistant Professor of Civil and Environmental Engineering, NJIT

Dr. Paul Chan, Committee member — Date
Professor of Civil and Environmental Engineering, NJIT

Dr. Robert Dresnack, Committee member — Date
Professor of Civil and Environmental Engineering, NJIT

BIOGRAPHICAL SKETCH

Author: Viriya Vithayaveroj

Degree: Master of Science in Environmental Engineering

Date: January 2000

Undergraduate and Graduate Education:

- Master of Science in Environmental Engineering,
  New Jersey Institute of Technology,
  Newark, NJ, 2000

- Bachelor of Engineering in Environmental Engineering,
  Chulalongkorn University,
  Bangkok, Thailand, 1998

Major: Environmental Engineering

This Thesis is dedicated to
my beloved family

ACKNOWLEDGEMENT

I would like to take this opportunity to express my appreciation to my advisor, Dr. Yuan Ding, for her guidance and inspiration. I would also like to express my sincere gratitude to my thesis committee members: Dr. Robert Dresnack and Dr. Paul Chan for their invaluable time and insightful advice.

I am indeed grateful to Ms. Annette Damiano and my friend, Sita Mohan, for their help.

I thank my parent, relatives, and friends for their supportive and sincere attitude.

TABLE OF CONTENTS

TABLE OF CONTENTS
(Continued)

Chapter **Page**

LIST OF TABLES

Table **Page**

LIST OF FIGURES

Figure **Page**

LIST OF FIGURES
(Continued)

Figure **Page**

CHAPTER 1

INTRODUCTION

1.1 Background

Colloidal particles are ubiquitous in an aquatic system. Due to this large specific area, colloidal particles carry a large amount of heavy metal and toxic organics. The removal of toxic colloidal particles is of critical importance in any environmental remediation work. The microcarrier process, a recent development which has been systematically developed by Ding *et al.*(1999) at NJIT through a grant funded by the USEPA. This process, in essence, applied the concept of flocculation with the sedimentation enhancement by microcarrier. From the operational point of view, the structural interaction between the flocs and the microcarrier plays an important role in controlling the mixing process.

Flocculation is one of the most common physico-chemical processes used in water and wastewater treatment in order to remove impurities in particulate form. The removal efficiency depends upon particle size and can be enhanced by aggregation of fine particles. The various terms of aggregation process known as agglomeration, agglutination, coagulation, or flocculation are used in different ways depending upon the area of application and the aggregation mechanism. Because of the lack of agreement on the differentiation between coagulation and flocculation, flocculation would be used here to cover all aggregation process.

Flocculation can be considered as a two-step process: (a) the destabilization of colloidal particles occurred by means of introducing appropriate chemical coagulants in

rapid mixing stage, and (b) the slow mixing stage in which the destabilized particles must be transported, collided, and formed into large stable clusters. These clusters, which form as the products of the process, are called flocs or aggregates. Thus, the structure of these flocs is of significant importance on the efficiency of the process. A review of the currently available literature indicates that very little work has been performed or reported. The objective of this thesis is to describe size and structure of microcarrier and the flocs obtained from the weighted flocculation process by using the Environmental Scanning Electron Microscope (ESEM). The following paragraphs present a literature review of the analytical aspect of flocculation mechanisms.

1.2 Colloidal Interactions

When two colloidal particles approach each other, several types of interactions can occur and they may have major effects on the flocculation process. Colloid interactions can influence flocculation by collision efficiency and the strength of aggregates. The two important kinds of colloidal interaction are van der Waals attraction and electrical repulsion that form the basis of the DLVO theory of colloid stability, proposed independently by Deryagin and Landau and Verwey and Overbeek. The stability of colloids depends on the attractive force and repulsive force between particles. If the attractive force is greater than the repulsive force, the particles will stick together and aggregation does occur. However, the other types of interaction such as hydration effects, hydrophobic interaction, steric interaction, polymer bridging, etc. are also important in many cases.

1.2.1 Van Der Waals Interaction

Van der Waals forces are the universal attractive forces between atoms and molecules and also between macroscopic objects. These forces play an important role in colloidal interaction. There are two approaches to calculate van der Waals force between macroscopic bodies: the Hamaker approach and the Lifshitz approach.

The Hamaker approach is obtained by assumping the pairwise additivity of over all interaction forces between two particles. Spontaneous electric and magnetic polarizations are considered to produce these interactions and give a fluctuating electromagnetic field within the media and in the gap between them. Lifshitz developed an expression for the interaction between two semi-infinite media separated by a plane-parallel gap **[1]**. According to the limitation of detailed information and the dielectric responses of the interacting media, the Hamaker approach is still widely used.

For two spherical particles, radii a_1 and a_2, separated by a distance d, the interaction energy is:

$$V_A = -\left(\frac{A_{12}}{6d}\right)\left(\frac{a_1 a_2}{a_1 + a_2}\right)$$

Where V_A is the attraction energy between the two spheres.

A_{12} is the Hamaker constant for interacting media.

In case of identical spheres of radius a_1, the interaction energy is:

$$V_A = -\frac{A_{11} a_1}{12d}$$

Where A_{11} is the Hamaker constant for medium 1.

In aqueous dispersions, Hamaker constants are in the range 0.3 to 10×10^{-20} J. The values of high-density materials are approximately the upper end of this range, while low-density materials, especially biological, have quite low values. The Hamaker expressions are employed only when the particles are at very close approach to each other. There is an inaccuracy when the separation distance is greater than 10% of the particle radius. For particle sizes larger than 1 μm, a correction for retardation is required. The retardation effect results from the electromagnetic character of van der Waals interaction. This effect is included in the Lifshitz approach and can be introduced into the Hamaker expressions by a simple empirical factor such as $1/(1+12d/\lambda)$ for spherical particles **[2]**. The retarded attraction between two identical spheres is given by

$$V_A = -\frac{A_{11}a_1}{[12d(1+12d/\lambda)]}$$

1.2.2 Electrical Interaction

In aqueous systems, all particles carry a surface charge that can be increased by various reasons, such as ionization of surface groups and specific adsorption of ions. When the particle surface is charged in an electrolyte solution, some of oppositely charged ions, known as counter ions, become attached to the surface. They are held together by strong electrostatic attraction and van der Waals forces that are sufficient to overwhelm thermal agitation. This is known as the Stern layer. This fixed layer surrounded with the remaining counter ions, which are distributed more broadly in a diffuse layer. The surface charge on a particle and the associated counter ion charge together constitute the

electrical double layer. A widely accepted double layer model is by virtue of Stern and modified later by Graham **[3]**.

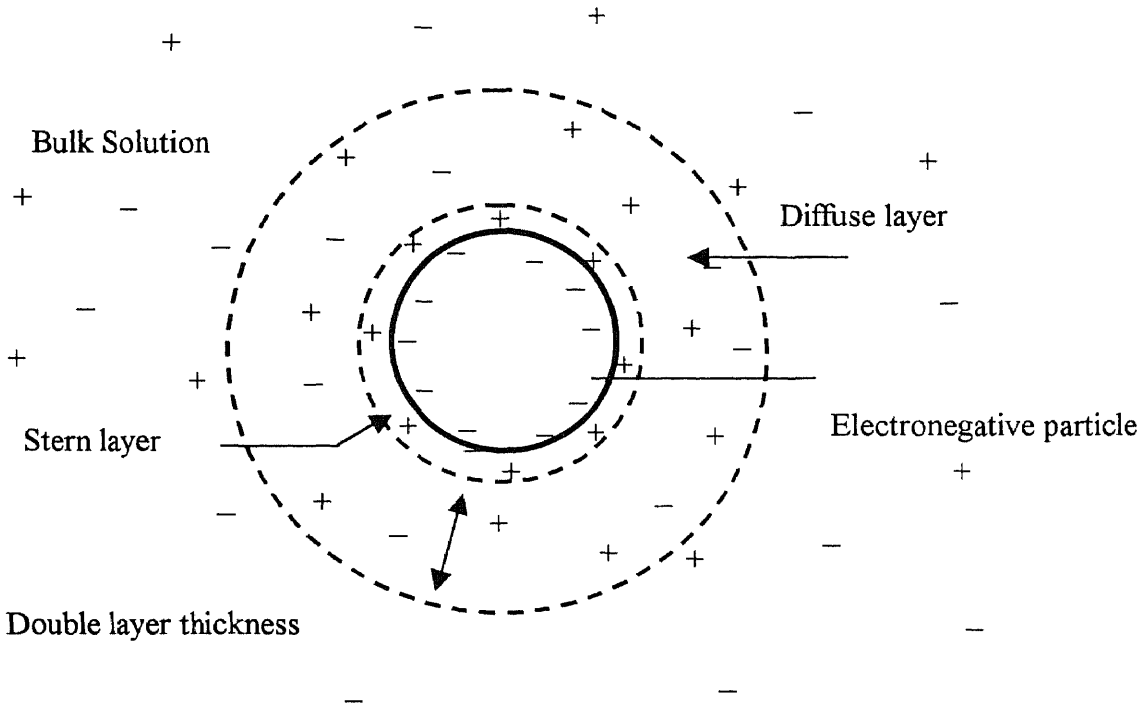

Figure 1.1 Schematic Illustration of a Negatively Charged Colloid Particle with Its Associated Electrical Double Layer **[28]**.

Figure 1.2 shows the effect of electrolyte concentration on the distribution of potential in the double layer for the case of (a) low, (b) high concentration of indifferent electrolyte and (c) a salt with a specifically adsorbed counterions giving charge reversal. The interaction between charged particles is conducted mainly by the overlap of diffuse layers. The two major effects on electrical interaction between particles are the magnitude of the effective surface potential and the extent of the diffuse layer; both of them depend on the ionic strength.

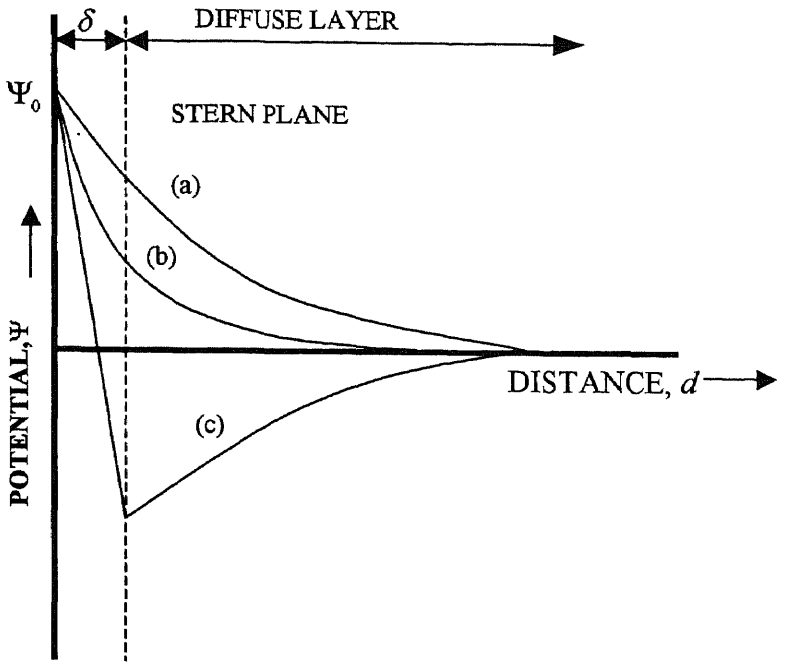

Figure 1.2 The Stern Model of the Electrical Double Layer, Showing the Variation in Potential with Distance from a Plane Charged Interface **[3]**.

The extent of the diffuse layer depends upon the ionic strength. The following equation is obtained for fairly low potentials in which the linear form of the Poisson-Boltzmann approach is appropriate **[4]**.

$$\psi = \psi_\delta \exp(-\kappa x)$$

Where ψ is the potential at a distance x from the Stern plane.

κ is the Debye-Huckel parameter, which is of great importance in colloid stability.

For aqueous solutions at 25°C, κ is given by

$$\kappa = 2.3 \times 10^9 \left(\sum c_i z_i^2 \right)^{1/2}$$

Where c_i is the molar concentration.

z_i is the valence of ion i.

The sum is taken over all ions present in solution.

When two identical charged particles in an electrolyte approach each other, their diffuse layers overlap and repulsion does occur between them. This repulsive energy can be computed in two methods. First method is by solving the Poisson-Boltzmann equation but this method usually result in an unanalyzable solution. The second method is by constructing the formula from known expressions for each of the surfaces involved.

For identical spheres, the Linear Superposition Approximation LSA result for the interaction energy is **[5]**:

$$V_E = 32\pi\varepsilon a \left(\frac{kT}{ze} \right)^2 \gamma^2 \exp(-\kappa d)$$

Where ε is the permittivity of the charge.

e is the elementary charge.

z is the valence of the ions.

γ is the dimensionless function of the surface function (zeta potential).

$$\gamma = \tanh\left(\frac{ze\varphi_0}{4kT} \right)$$

Increasing ionic strength has two effects on electrical double layer interaction. As the Debye-Huckel parameter (κ) increases, the range of repulsion decreases. In effect, particles may approach closer before they repel each other. The second effect is the reduction of the repulsion at a given separation distance. This is resulted from the decrease in the zeta potential of particles from the added salt. Generally, highly charged counter ions have the greatest effect **[6]**.

1.2.3 Hydration Effects

For various reasons, the nature of water adjacent to a particle surface can be very different from the ordinary, bulk water. As most particles have surface charge, therefore ionic groups, some hydration of these groups would be calculated. At closer approach of two hydrated surface particles, an extra repulsive interaction, hydration force, becomes important. This interaction will prevent the contact between those particles regarding to the tendency to be dehydrated.

In the measurements of the force between mica sheets in various electrolyte solutions **[7]**, the repulsion would follow the expected exponential form for double layer interaction until the salt concentration is above 1 mM; an extra short-range force manifests. This force increases with the degree of hydration of the adsorbed hydrated cations ($Li^+ = Na^+ > K^+ > Cs^+$) and decreases exponentially over the range 1.5 to 4 nm, with a decay length of the order of 1 nm.

The range of hydration forces is greater than the range of double layer repulsion. They might have significance on colloid stability, especially at high ionic strength.

1.2.4 Hydrophobic Interaction

In aqueous system, there are two broad kinds of material: hydrophilic and hydrophobic colloids. Hydrophilic colloids are water-soluble materials, which are thermodynamically stable. In the presence of chemical changes or changes in temperature, they can agglomerate together. In contrast to hydrophilic colloids, the solubility of hydrophobic colloids is low. The particles have kinetic stability due to repulsive force between particles, although they are unstable thermodynamically. As a result, the formation of permanent aggregates is hindered. However, hydrophobic particles may have a hydrophilic surface by moistening with water **[8]**.

Hydrophobic interaction arises from hydrogen bonding between the molecules, which is responsible for a substantial degree of association between water molecules and a significant structuring effect. A hydrophobic surface has no affinity for water because of the lack of hydrogen-bonding sites. When this surface exists, the structuring tendency of water will limit by preventing the hydrogen bond formation in certain directions. As a result, water would escape from such surfaces. In aqueous solutions, hydrophobic portions on the molecules will attach to each other to decrease interactions between water and the hydrophobic regions. This is known as hydrophobic bonding. It was found that this attraction was much stronger and broadly range than the van der Waals force **[9-10]**.

1.2.5 Steric Interaction

Steric effects have significance in systems containing uncharged particles with adsorbed macromolecules **[11]**. Large amount of absorbed polymer can give greatly enhanced stability by a steric stabilization. In the case of small adsorbed amounts, a bridging

mechanism takes place to promote flocculation. The most effective stabilizers are polymers that have some affinity for the surface but can adsorb with some segments on polymer chains and with loops and tails extending into solution. When particles approach close enough, the adsorbed layers come into contact. Some overlap of the hydrophilic chains is involved. As these chains are hydrated, the overlap causes some dehydration and, therefore, the free energy and repulsion between particles increase. The adsorbed layer can give hydrophobic particles some of the important properties of hydrophilic colloids **[12]**.

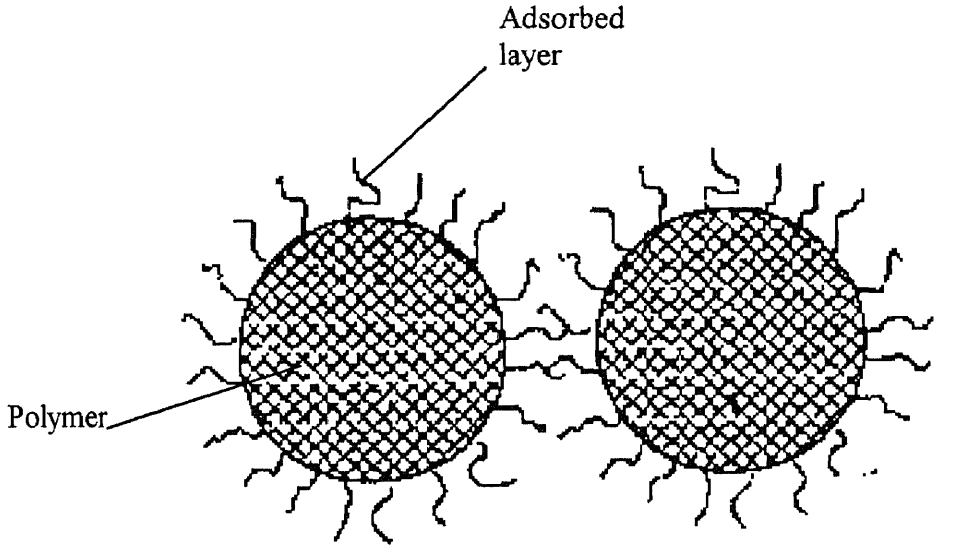

Figure 1.3 Steric Interaction of Particles with Adsorbed Polymer Chains **[15]**.

The thickness of the adsorbed layer also plays an important role in determining the stabilizing effect. The natural organic materials **[13]**, such as humic substances, are always present in the adsorbed layers of most particles in the aquatic system. These

materials can have an important effect on their colloidal behavior. Humic substances are known to enhance the stability of inorganic colloids **[14]** and can cause greatly increased flocculant dosages.

1.2.6 Polymer Bridging

Several substances in nature, such as starch, cellulose, some types of sugar, and some types of protein, including the organic polymer that is synthesized, can be used as coagulants in a colloid removal process. These organic substances have quite high molecular weights. The organic polymer can have positive charge, negative charge, or neutral charge.

In polymer bridging, the molecules of polymer can attach to colloid in several positions. The attachment may results from the different charges of polymer and colloid or the attractive force from the chemical reaction, which occur between the same charges of polymer and colloid. The polymer bridging can occur when polymer and vacant space on the particle surface are present. The individual chain, which remains free of adsorbed polymer, can stick with other particles by bridging them together.

An optimum dosage is required for effective flocculation for each solution. If the adsorbed polymer is not enough, bridging links between particles can not be formed. On the other hand, an excess absorption of polymer prevents the bridging links as there is insufficient free particle surface for bridging contacts to occur and the adsorbed layer may cause steric repulsion. Bridging flocculation gives much larger and stronger aggregates than those produced by simply reducing electrical repulsion **[15]**.

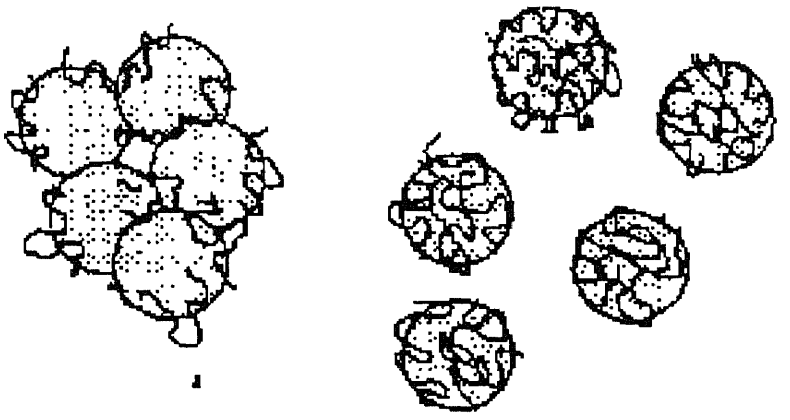

(a) (b)

Figure 1.4 Schematic Illustration of (a) Bridging Flocculation and (b) Re-Stabilization by Adsorbed Polymer Chains **[15]**.

Since the reversal of local charge and unoccupied surface area are available on the original charged particle, the polyelectrolyte which has a higher charge density than the particle surface can adsorb on an oppositely charged particle in a manner of presence in patches of excess charge. This mechanism is the so-called electrostatic patch effect **[16]**. Particles with polymer adsorbed in this patchwise manner can interact in such a way that oppositely-charged areas of different particles are adjacent. Consequently, the strong attraction is given. This can be considered as another form of bridging interaction.

1.2.7 Combined Interaction-Colloid Stability

Exclusively, Deryagin and Landau **[17]** and Verwey and Overbeek **[18]** developed the DLVO theory of colloid stability. This is formed by means of Van der Waals attraction

and electrical double layer repulsion, assuming that these interactions are additive and be combined to give the total interaction energy between particles as a function of separation distance.

The following equation describes the total interaction energy between two equal particles:

$$V_T = 32\pi\varepsilon a\left(\frac{kT}{ze}\right)^2 \gamma^2 \exp(-\kappa d) - \left(\frac{Aa}{12d}\right)$$

When the repulsive force overcomes the attractive force, a potential energy barrier occurs. This barrier would keep particles away from each other and also prevent aggregation. However, the energy barrier would be lower and leading to aggregation as a result of increasing of ionic strength or reduction of the zeta potential. As the barrier is overwhelmed, the particles are held strongly by van der Waals force in an infinite primary minimum depth.

At sufficiently large separation distances, the attractive force would be greater than the repulsive force and hence aggregation could occur without the particles coming into close contact. This is called a secondary minimum in the potential energy curve. The relationship between interaction energy and separation distance is shown in figure 1.5.

The addition of salt brings about increasing the ionic strength and reducing the zeta potential. At this point, the barrier height disappears and the following condition applies:

$$V_T = 0$$

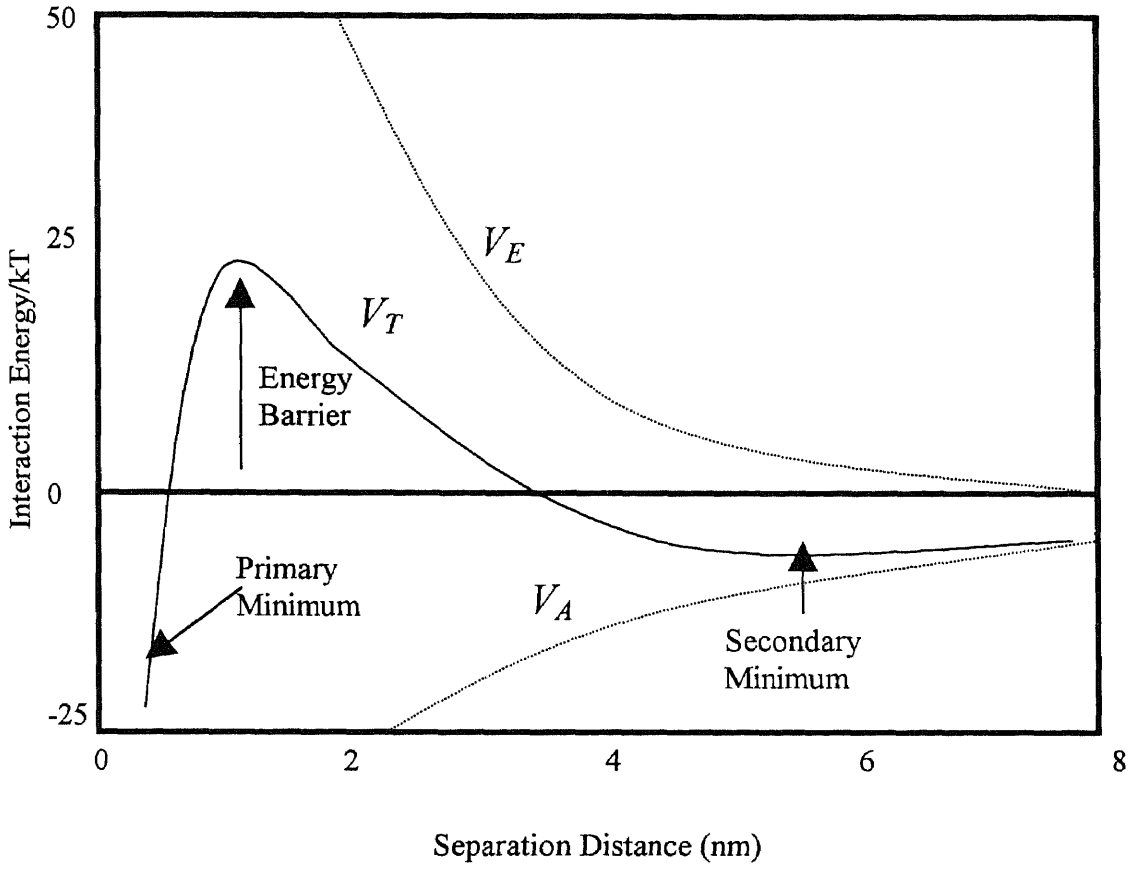

Figure 1.5 Schematic Illustration of Electrical (V_E), Van der Waals (V_A), and Total (V_T) Interaction Energies between Equal Spherical Particles as a Function of Separation Distance **[15]**.

Under this condition, the critical flocculation concentration, c_f, for a symmetrical electrolyte becomes:

$$c_f = K\left(\frac{\gamma^4}{A^2 z^6}\right)$$

Where K is a constant which depends upon the properties of the dispersion medium.

A is the appropriate Hamaker constant.

It is found that when zeta potential is very high, the term γ approximates unity and c_f becomes inversely proportional to the sixth power of the valency, z. This dependence of c_f on $1/z^6$ is known as the Schulze-Hardy rule, in which the counter ion charge has the important effect **[19]**. However, there are a few evidences in which the inverse sixth power law is observed.

The full destabilization can be accomplished at low ionic strength by having the zeta potential decrease to the critical value. If the additive ionic strength is increased, the zeta potential can be reversed and the particles turn to stable again. This process is known as restabilization.

1.3 Flocculation Kinetics

The following equation is the Smoluchowski approach, the rectilinear model of the aggregation of heterodisperse suspension, by assuming aggregates are coalesced spheres.

$$\frac{dn_k}{dt} = \frac{1}{2}\sum_{i+j=k} \alpha_a \beta(i,j) n_i n_j - n_k \sum_{alli} \alpha_a \beta(i,k) n_i$$

Where the subscripts i, j, and k refer to different sizes of particles.

n_i, n_j ,and n_k are the number concentrations of particles of size i, j, and k, respectively.

$\beta(i,j)$ and $\beta(i,k)$ are mass transport coefficients describing collisions between particles of the size classes indicated.

α_a is a stability factor, the ratio of the rate at which particles attach to the rate at which particles collide.

The term on the left-hand side of equation represents the change in number concentration of particles of size k with respect to time. The first term on the right-hand describes the formation of particles of size k by collision between particles of sizes i and j. The second term describes the losses of particles of size k by collision between any other size **[20]**.

1.3.1 Collision Frequency Factor

Interparticle contacts can be carried out in 3 distinct particle transport mechanisms: Brownian motion, velocity gradients, and differential settling **[21]**.

When Brownian motion dominates particle transport, the mass transport depends upon thermal and viscous effects only. The mass transport coefficient, $\beta_{bd}(i,j)$, becomes:

$$\beta_{bd}(i,j) = \frac{2kT(d_i + d_j)^2}{3\mu d_i d_j}$$

Velocity gradients are present in all fluid flows, either laminar or turbulent. Particle transport depends upon the mean velocity gradients in the fluid, G (s^{-1}). The mass transport coefficient, $\beta_{vg}(i,j)$, becomes:

$$\beta_{vg}(i,j) = \frac{1}{6}(d_i + d_j)^3 G$$

a. Brownian Motion

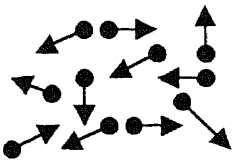

b. Velocity gradients

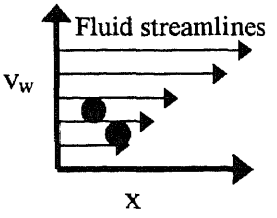

c. Differential settling

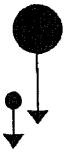

Figure 1.6 Schematic Illustration of Rectilinear Models for the Transport of Suspended Particles in Aquatic Systems **[22]**.

Differential settling is influenced by gravity force, which brings about settling of particles and depends on the buoyant weight of the particles. Large or dense particles can contact smaller or less dense ones in a process. The mass transport coefficient, $\beta_{ds}(i,j)$, becomes:

$$\beta_{ds}(i,j) = \frac{\pi g}{72\mu}(\rho_p - \rho)(d_i + d_j)|d_i - d_j|$$

Assuming that the mechanisms of particle transport are independent, the mass transport for submicron particles can be determined as the following equation.

$$\beta(i,j) = \beta_{bd}(i,j) + \beta_{vg}(i,j) + \beta_{ds}(i,j)$$

Regardless of the hydrodynamic interactions and short range forces between approaching particles in the Smoluchowski approach, the aggregation rate would be overpredicted. The coalesced sphere assumption underpredicts the actual collision rates that take place **[23]**.

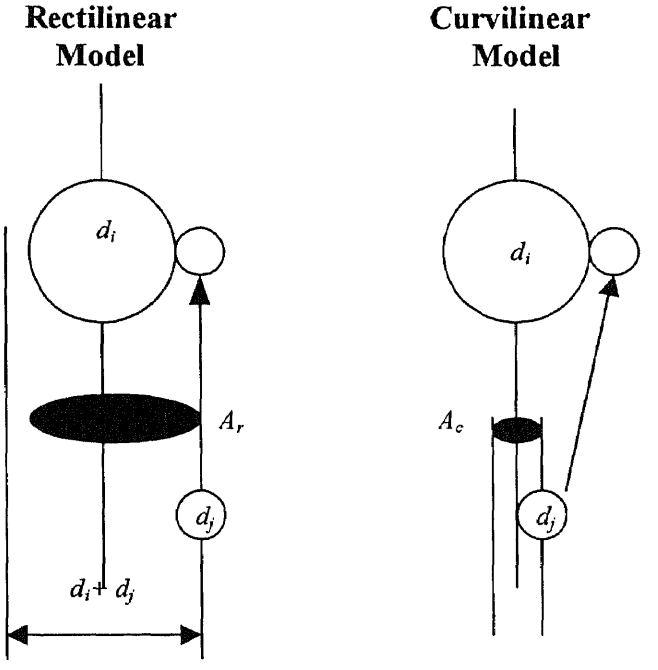

Figure 1.7 Schematic Illustration of the Difference between Rectilinear and Curvilinear Trajectories in Particle Transport by Differential Settling **[25]**.

The differences between the rectilinear and curvilinear approaches for transport by differential settling are illustrated schematically in Figure 1.7 adapted from Han and Lawler **[24]**. In the rectilinear model, all d_j-size particles residing within the shaded area, A_r, can come to attach the d_i-size particle. Under the curvilinear approach, all

hydrodynamic interactions are considered. Only the small particles in the shaded area, A_c, can come to attach to the large one. As a result, the actual collision rate is less than the rectilinear rate. The actual mass transport coefficient becomes $[(A_c/A_r)\ \beta_{ds}(i,j)]$.

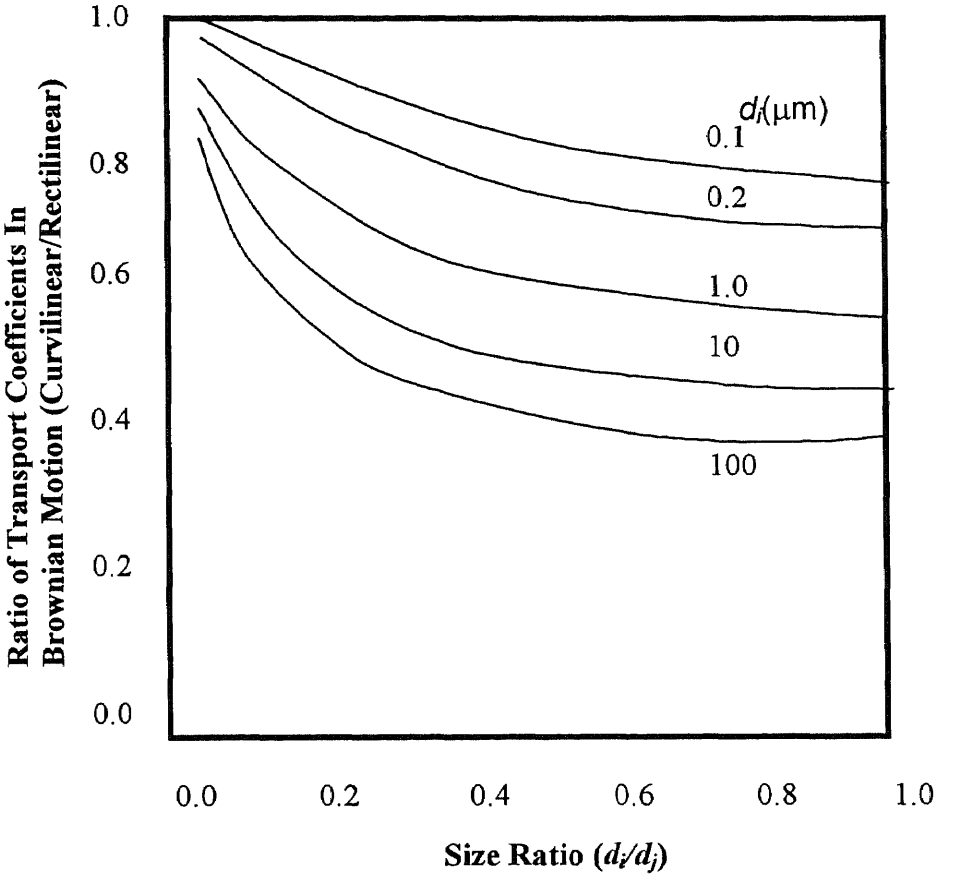

Figure 1.8 Effect of Particle Size on Mass Transport Coefficients in Brownian Motion [25].

The effects of hydrodynamic interactions on particle transport by Brownian motion are shown in Figure 1.8. In these calculations, van der Waals forces are included as the separating distance between particles reduces. The reduction of the transport rate relative to the rectilinear approach for monodisperse suspensions ($d_i/d_j \rightarrow 1$) is more than

for heterodisperse suspensions ($d_i/d_j << 1$). A dimensionless group, H_A, characterizes the effects of particle size, velocity gradient, and van der Waals interaction as follow:

$$H_A = \frac{A}{18\pi\mu d_j^3 G}$$

Where A is the Hamaker constant.

d_j is the diameter of the larger of two interacting particles.

Under the velocity gradient condition, hydrodynamic interactions are insignificant for monodisperse suspensions and turn to be significant when the systems become heterodisperse. Increasing the velocity gradient or the size of particles increases the interaction and the deviation from the rectilinear approach. This yields H_A with smaller values as the hydrodynamic effects become more substantial.

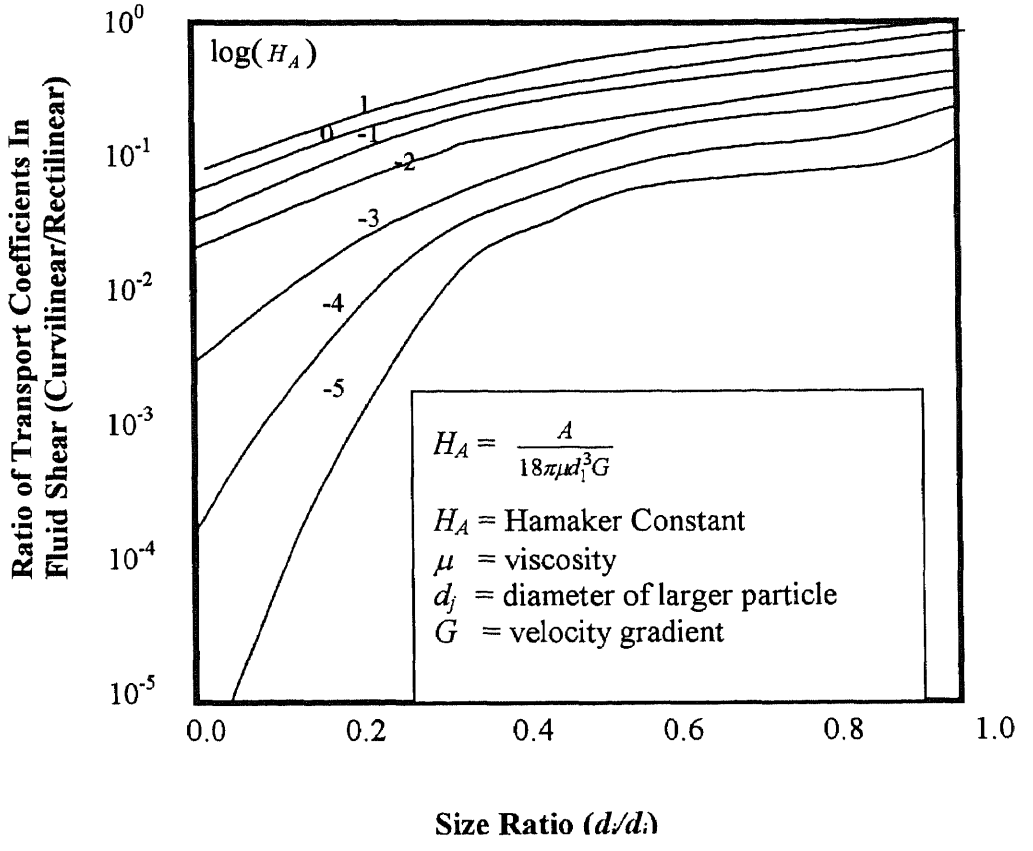

Figure 1.9 Effect of Particle Size on Mass Transport Coefficients in Fluid Shear **[25]**.

1.3.2 Collision Efficiency

Due to the presence of the potential energy barrier, only some collisions are successful. The ratio of the experimental aggregation rate to fastest rate observed is known as the collision efficiency factor, α_a, defined as follows:

$$\alpha_a = \frac{rate\ at\ which\ particles\ attach}{rate\ at\ which\ particles\ collide}$$

The colloidal stability of particles can also be described by a collision efficiency factor.

In a completely stable suspension, repulsive interactions are significant. Hence all collisions are unsuccessful and $\alpha_a = 0$. In contrast, for a completely unstable suspension, repulsive interactions are insignificant, all collisions yield aggregation and $\alpha_a = 1$.

Based on the transport process, several investigators have used two kinds of experimental studies. For particles larger than a micron, Brownian motion is insignificant. The considerable-controlled velocity gradients are applied in the experiments to yield the describable interparticle contact rates. For submicron particles, Brownian motion controls interparticle contacts, and Smoluchowski's theory of perikinetic flocculation or a suitable modification is used to describe interparticle contacts for both monodisperse and heterodisperse suspensions **[26]**.

When particles undergo velocity gradient, the collision efficiency factor becomes:

$$\alpha_a = \frac{\pi}{4\phi G t} \ln \frac{n_o}{n_t}$$

Where n_o and n_t are the number concentrations of particles at the beginning and at time t of the experiment, respectively.

ϕ is the constant volume fraction of solid material in the suspension.

1.4 Flocculating Agents

1.4.1 Metal Ion Salts

The main reasons for selecting flocculating agents are cost, effectiveness,and its capability of multicharged polynuclear complexes formation with enhanced adsorption properties in aqueous systems **[27]**. According to the Schulze-Hardy rule, iron and aluminum salts are two widely used flocculants in the water and wastewater treatment

[28]. The commonly used iron and aluminum salts are ferric sulfate, ferrous sulfate, ferric chloride, aluminium sulfate, aluminium chloride, polyalumimium chloride (PAC), and sodium aluminate.

When iron or aluminum salts is introduced to the process, the trivalent ferric or aluminum ion will hydrate to form coordination compounds $Fe(H_2O)_6^{3+}$ and $Al(H_2O)_6^{3+}$. These compounds then undergo hydrolysis reactions yielding metal (M) hydroxo complexes species $[M(H_2O)_5OH]^{2+}$, $[M(H_2O)_4(OH)_2]^{+}$, $[M_6(OH)_{15}]^{3+}$, $[M_8(OH)_{20}]^{4+}$, $M(OH)_3$ (s), $[M(OH)_4]^-$. The pH is the controlling factor of these hydrolysis products and the precipitation of metal hydroxides.

1.4.2 Polymeric Flocculants

Most of the polymeric flocculants used are long chain synthetic organic compounds, however, some natural products such as starches and extracts from various types of seed can also used as flocculating agents. Polymeric flocculants are classified into three groups, based on the local surface charge of flocculant: cationic, anionic, and nonionic [29].

Cationic polymers are very effective to remove negatively charged colloids by absorption and neutralization of local charge. Therefore, this kind of polymer is not needed to have a high molecular weight. Flocs formed by charge neutralization are stronger than those formed by simple salts.

On the other hand, anionic and nonionic polymers must have molecular weights greater than one million in order to bridging the potential energy barrier between two negatively charged colloids. The required molecular weight is dependent on the number

of charged group, degree of branching of the polymer, charge on the colloid, and ionic strength of solution **[30]**. Anion polymer is ineffective when it is used as a flocculating agent alone to remove negative charged particles. It will be effective just after the extraneous electrolytes such as divalent metal ions are added to the process. The divalent metal ion, such as calcium and magnesium ions, help an anionic polymer to encourage its ability to absorb negative colloids. It was found that charge density is another important factor as well as molecular weight. Any change in ionic strength of solution will affect the shape of polymer molecules and bridging formation of a charged polymer.

1.5 Weighted Flocculation

The settling rate of floc resulting from flocculation has been known to be rather slow in wastewater treatment due to their low specific gravity. In order to remove these small particles, a large detention tank would be required to accommodate the high discharge rate, e.g. stormwater runoff. The weighted flocculation approach has been explored by a number of industries, e.g. the Microsep® (International water Solutions Corporation), the Actiflo® (Omnium de Traitement et de Valorisation [OTV]), and DensaDeg® (Infilco Degremont, Inc.), aiming to enhance the sedimentation rate. Unfortunately, a review of the current available literature indicates that there is a lack of systematic studies of this subject. And, in fact, the conventional jar test was found to be deficient, if not impossible, to evaluate the performance of the weighted flocculation. A modified jar test recently developed by Ding *et al.* **[33]**, was designed to maintain the integrity of the floc-microcarrier structure by minimizing shear breakage. Details of the test device are presented elsewhere by Ding *et al.* **[33]**.

Microsand has been used as a weighted carrier of colloidal particles. This process was developed and applied to drinking water supply. It is increasingly being used for treating combined wet-, dry-weather flow (WWF/DWF), CSOs **[35-36]**, and wastewater.

Guibelin *et al.* **[37]** developed the Actiflo® process for stromwater treatment. This process combined lamellae settling with the weighted flocculation. Microcarrier and coagulants have been added into a mixing chamber that are followed by flocculation and sedimentation tanks. The initial reaction of the flocculation process is improved by presence of the microcarrier and polyelectrolyte, which increases the bonding of the floc to the microcarrier, resulting in higher settling velocities. Above 80% of total suspended solids was gained by using 60 g/m^3 of ferric chloride and 0.8 g/m^3 of polyelectrolyte at the upflow velocity of 130 $m^3/h/m^2$.

De Dianous and Dernaucourt **[38]** compared conventional flocculation with weighted flocculation using microsand in water treatment. This study has shown that the weighted floc is more cohesive. Hence, it has a higher velocity gradient and less contact time. The settling velocity is also 5 times higher than that of unweighted floc. Furthermore, the microsand is recyclable. Because of the good results, the above researchers had used this method on an industrial scale, which is characterized by a contact time of 8 minutes and an upflow velocity of 40 $m^3/h/m^2$.

1.6 Fractal Geometry

The structure of a floc is described in term of fractal geometry because of its irregular and disordered nature. The fractal theory was developed by Mandelbrot **[39]** providing a complete approach to characterize many natural and engineering systems that have

irregularity or indefinite form. The important characteristic of fractals is self-similarity, which means their morphology is invariant to a change of length scale. The most important numerical parameter in fractal theory is the fractal dimension, D_f **[41-43]**. The fractal dimension can be defined in relation to changes in packing density, connectivity between component particles, surface area, velocity distributions in turbulent fluids, and other characteristics of an object that are observed to have special scaling properties **[40]**.

For aggregates, the fractal dimension measures how the particles occupy the space in the aggregate. The following equation shows the relationship between the mass, $M(R)$, and the size of aggregate, R:

$$M(R) \propto R^{Df}$$

In general, the fractal dimensions are in a range of 1.7-1.8 under diffusion limited aggregation (DLA) conditions and 2.2-2.3 under reaction limited aggregation (RLA).

Under diffusion limited aggregation (DLA), there is no repulsion between colliding particles. The particle transport in Brownian motion and that of each collision leads to aggregation. In reaction limited aggregation (RLA), an inter-particle repulsion occurs, the collision efficiency is reduced and all collisions do not subject to aggregation. The particles have to collide many times before cluster. Greatly different aggregate structures can be obtained under this condition.

There have been a number of experimental studies on the structure of various kinds of floc through computer modeling **[44-47]**, various scattering techniques **[48-52]**, dynamic scaling **[52-53]**, and image analysis from microscopes **[54-59]**.

An early work in the area of study in electron microscopy for small aggregated particles was carried out by Forrest and Witten **[54]**. They examined smoke-particle

aggregates through the micrograph. The results showed the existence of long-range correlation, which follow a power law.

Tence *et al.* **[55]** used the digital annual dark-field imaging in a Scanning Transmission Electron Microscope (STEM) to measure the fractal dimension of aggregated iron polydisperse particles and compared the results with those obtained through computer modeling of a polydispersed system in a cluster-cluster aggregation process. The results showed strong visual similarity between the experimental and simulated images for the Gaussian-like size distribution and cluster-cluster aggregation with linear trajectories. This is confirmed by the value of fractal dimension (D_f = 1.9± 0.1). In addition, it was found that polydispersity does not affect the fractal dimension.

As the Confocal Scanning Laser Microscopy (CSLM) appeared to be rather powerful since it provides direct information, Bremer *et al.* **[56]** used this technique to analyze the structure of particle gels. The fractal dimensions of casein and polystyrene obtained from various techniques were similar comparing to the experimental results (D_f = 2.35). In order to diminish the disturbing effect of sedimentation to the gel formation, the microgravity should be reduced.

Pierre *et al.* **[57]** studied the structure evolution of kaolinite flocs during their formation in aqueous medium under a Scanning Electron Microscope (SEM) by hypercritical drying with liquid CO_2, as a function of Fe electrolyte content. The results showed that particles consistently formed the floc with diffusion limited aggregation (DLA) in the presence of Fe electrolytes. On the other hand, a uniformly porous accumulated sediment was formed under gravity force in the absence of Fe electrolytes.

Zhang and Buffle **[58]** determined the fractal dimension of KCl-induced hematite aggregates using three different approaches: dynamic scaling, Transmission Electron Microscopy (TEM) image analysis, and static light scattering (SLS). Under the diffusion limited aggregation (DLA) condition ([KCl] > 100 mM), the value of fractal dimension obtained from dynamic scaling, analysis of TEM images, and static light scattering were 1.87 ± 0.07, 1.68 ± 0.04, and 1.83 ± 0.07, respectively. In the regime of reaction limited aggregation (RLA), the aggregates are more compact. The compactness makes a difficult to determine the fractal dimension under TEM image analysis. The static light scattering analysis yields a fractal dimension of 2.20 ± 0.09 in this regime.

Cornelissen *et al.* **[59]** employed four types of microscopy techniques: Light Microscope (LM), Scanning Electron Microscope (SEM), Transmission Electron Microscope (TEM), and Atomic Force Microscope (AFM), to investigate the visual structural information of hydrous floc particles. These flocs were prepared by 2 different methods. The first method is a batch preparation that was performed by using a Jar test system. The second method is a continuous preparation, which was carried out by using a micro-scale flocculation system. It was found that hydrous flocs are fractal in nature but they will lose this property and become amorphous when their sizes are approximately 0.1-1 μm. The growth of the aggregates is difficult to control. The large (1-100 μm) flocs could be damaged without losing structural information, which is usually caused by drying the sample, when they were prepared by cryogenic freezing before observation under the SEM. Damage caused by drying was not apparent with the TEM technique used. It was shown that the various microscope techniques brought about compatible

results in the size range of 10 nm-5mm. The floc structure is more reproducible when using a micro-scale continuous flow system.

Snidaro *et al.* **[60]** described activated floc structure using four investigation methods: size distribution analysis associated with sonication, Transmission Electron Microscopy (TEM), Confocal Scanning Laser Microscopy (CSLM) and fractal dimension analysis, and three dimensional modeling. Under Confocal Scanning Laser Microscopy, a 13 μm aggregate was observed. It appeared that this aggregate is a fractal object and the total number of cells in the cluster was about 2^n number. These explained that the formation of 13 μm units were microcolonies. The predominant microflocs (125 μm) were the aggregates of microcolonies. Investigation by Transmission Electron Microscope showed that 2.5 μm units were bacteria, which formed 13 μm microcolonies. A gel-like matrix of exopolymer provides the cohesion of these aggregates. The mass fractal dimensions of microcolonies and microflocs are 3 and 2.5, respectively. These values showed that aggregation mechanisms are different: cell division for microcolonies and diffusion limited particle-cluster for microflocs.

Liang and Kendall **[61]** studied the aggregate formation of polystyrene latex (0.92 and 1.9 μm in diameter), concentrated cyclohexane in water emulsion (2.5 μm in diameter), and human red blood cells (5.7 μm in diameter) under conductivity counting method and microscopy method. The results showed that the aggregate size and volume increased with increase in particle volume fraction. The force that forms aggregates is a weak interparticle attraction. The adhesion energy is low and can be estimated from the aggregates peak size using a theoretical equation.

1.7 Objective

The objective of this thesis is to examine the structural interaction between the flocs obtained from the weighted flocculation process and the microcarrier by using the Environmental Scanning Electron Microscope (ESEM).

The experimental study includes the prescreening stage and the observation under the ESEM stage. The experiments in the first stage were carried out using electrolyte, polyelectrolyte, and microcarrier. The controlling parameter of the process was the turbidity. The structural relationship between microcarrier and flocs was observed under the Environmental Scanning Electron Microscope (ESEM) in the second stage.

CHAPTER 2

EXPERIMENTAL

2.1 Sample Preparation

The dry residual material was collected from the NJIT parking lot # 6 and used to prepare the synthetic sample. The material was sieved and divided into seven different size ranges. It was found that particles with grain size larger than 106 micrometers would settle too fast to make a uniform sample while particles with grain size smaller than that would remain suspended. It was concluded that particles smaller than 106 micrometers were more suitable for suspension.

2.2 Types of Coagulants

2.2.1 Electrolyte

Ferric chloride is one of the most widely use coagulants in the removal of colloid particles. The advantages of ferric chloride are its use in a broad pH range and it forms a heavy floc. Ferric chloride was used as an electrolyte in this study. Fe^{3+} solution was prepared by dissolving $FeCl_3 \cdot 6H_2O$ crystal in deionized water.

2.2.2 Polyelectrolyte

A 309C cationic polymer was selected to use as a polyelectrolyte. 309C (49%) from Polydyne Inc., Riceboro, Georgia, was dissolved in deionized water.

2.2.3 Microcarrier

Ottawa sand was used as a microcarrier in the weighted flocculation process. The size range of Ottawa sand used was between 53-75 micrometers by sieve analysis. All containers and the microcarrier were first washed thoroughly with a detergent and tap water, then rinsed 3 times with tap water to remove all traces of residual washing compound. Finally, the sand was rinsed with deionized water to ensure that no other particles were attached to the sand and involved in the process.

2.3 Instruments and Experimental Procedure

2.3.1 Jar Test Apparatus

The Jar Test has been widely used to determine the dosage and the effectiveness of various coagulants in water and wastewater treatment processes. In the conventional jar test, a series of six beakers are stirred simultaneously by paddle stirring after the addition of flocculant doses. A new jar test technology is using microcarrier to enhance the jar test efficiency due to its different physical conditions. A microcarrier weighted jar test that had been adopted in this study was developed by Dr. Yuan Ding, Department of Civil and Environmental Engineering, NJIT. The Jar Test apparatus consists of six 2000-mL square beakers and a laboratory stirrer with a speed drive range of 0-300 rpm (PB-700TM Jar tester, Phipps & Bird, Richmond, Virginia).

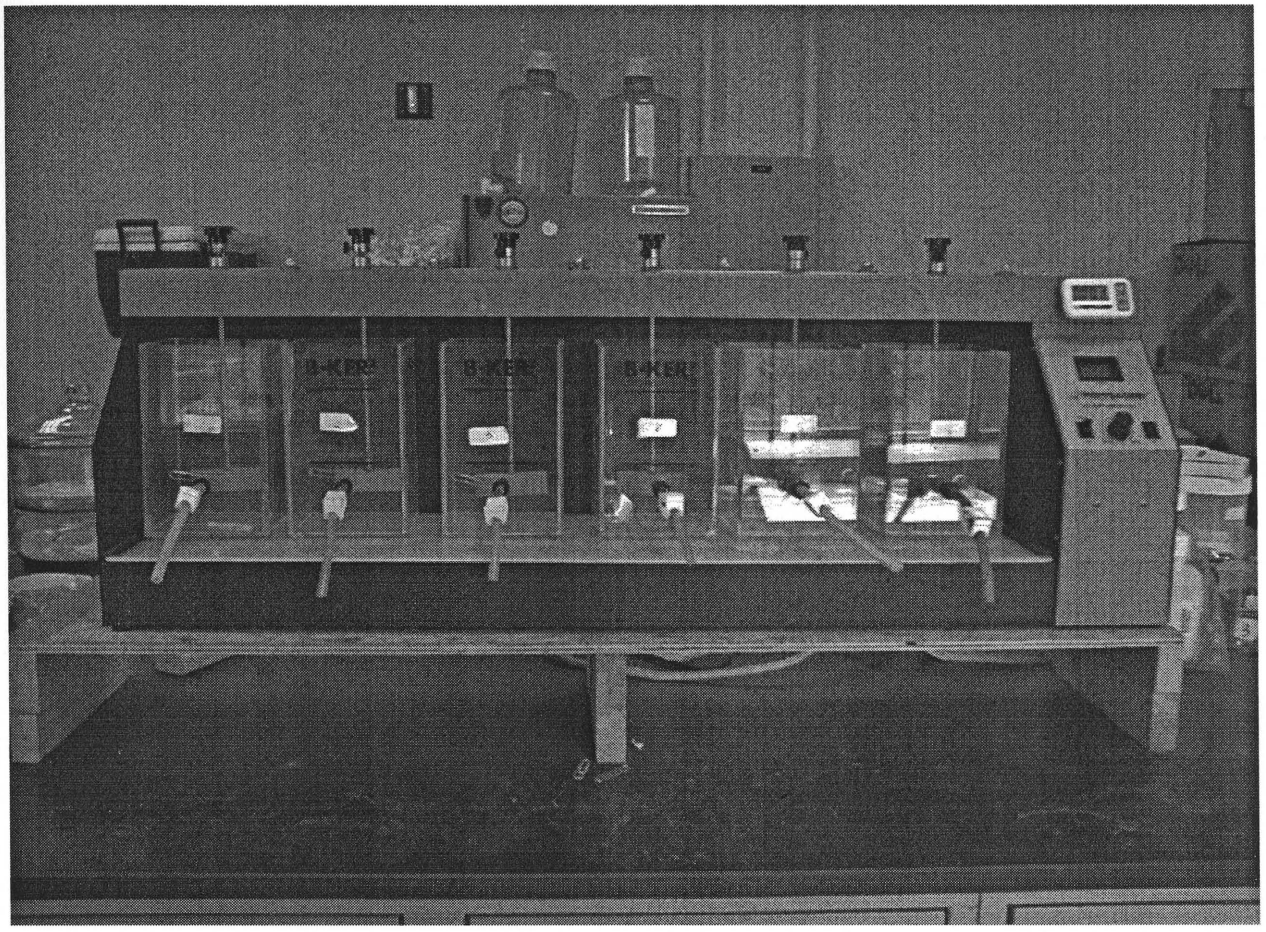

Figure 2.1 Jar Test Apparatus

The microcarrier weighted jar test procedures are as follows **[33]**:

1. Prepare a synthetic sample and analyze its turbidity.
2. Place 1000 mL of the synthetic sample into a 2000-mL jar on the six-jar laboratory stirrer and check the stirrer operation. A light table facilitates viewing of the contents of the beakers.
3. Dose the sample in each jar with predetermined amount of ferric chloride, polyelectrolyte, microcarrier, and sodium bentonite.
4. Operate at a rapid mixing rate of 150 rpm for 10 seconds.

5. Reduce the stirring rate to 100 rpm for 20 seconds and then to 60 rpm for 30 seconds for flocculating.
6. Remove the paddle and allow the solutions to settle for 3 minutes after flocculation.
7. Take the supernatant one inch below the surface of water in each jar to measure the turbidity and follow by taking sludge to investigate floc structure. Select the optimum dosage on the basis of supernatant clarity and settling of flocs.

2.3.2 Turbidimeter

Turbidity was measured by a HF Scientific DRT-15CE turbidimeter (HF Scientific Inc., Fort Myers, Florida). The measurement range is 0-1000 NTU (Nephelometric Turbidity Unit). This turbidimeter employs the principle of nephelometry. This method is based on a comparison of the intensity of light scattered by the sample with the intensity of light scattered by a standard reference suspension, formazin polymer, under the same conditions.

In the turbidimeter, a light source illuminates the sample and then one or more photoelectric detectors with the instrument meter will measure the intensity of scattered light at the right angle of the path of the incident light. The standard procedures to measure turbidity are as follows **[62]**.

1. Turbidity calibration: Formazin as a HF scientific factory certified secondary standard is used to calibrated HF turbidimeter. The available standard suspensions are 10, 100, and 1000 NTU. The reference standard is the standard suspension of 0.02 NTU, which is contained in the pre-selected cuvettes with light shield caps. The instrument should be calibrated using all the secondary standard solutions.

2. Measurement of turbidities less than 40 NTU: Shake the sample thoroughly. Wait until air bubbles disappear and pour the sample into the turbidimeter tube. Read the turbidity directly from the readout device or from the appropriate calibration curve.
3. Measurement of turbidities above 40 NTU: Dilute sample with one or more volumes of turbidity-free water until the turbidity falls between 30 and 40 NTU. Calculate the turbidity of original sample from the turbidity of the diluted sample and the dilution factor.

Figure 2.2 Turbidimeter

2.3.3 Environmental Scanning Electron Microscope

The images of dry residual material, microcarrier, and floc have been observed under the Environmental Scanning Electron Microscope (ESEM) Model 2020, LaB6, 0-50 Torr, ElectroScan Corporation. The ESEM was developed in order to transcend the limitations of the conventional SEM. It can use to investigate the sample material that are impossible to measure under the conventional SEM. Moreover, it has diminished the requirement for sample preparation. The important characteristics of ESEM are the multiple pressure limiting apertures, the graduated vacuum system, and the Environmental or Gases Secondary Electron Detectors (GSED).

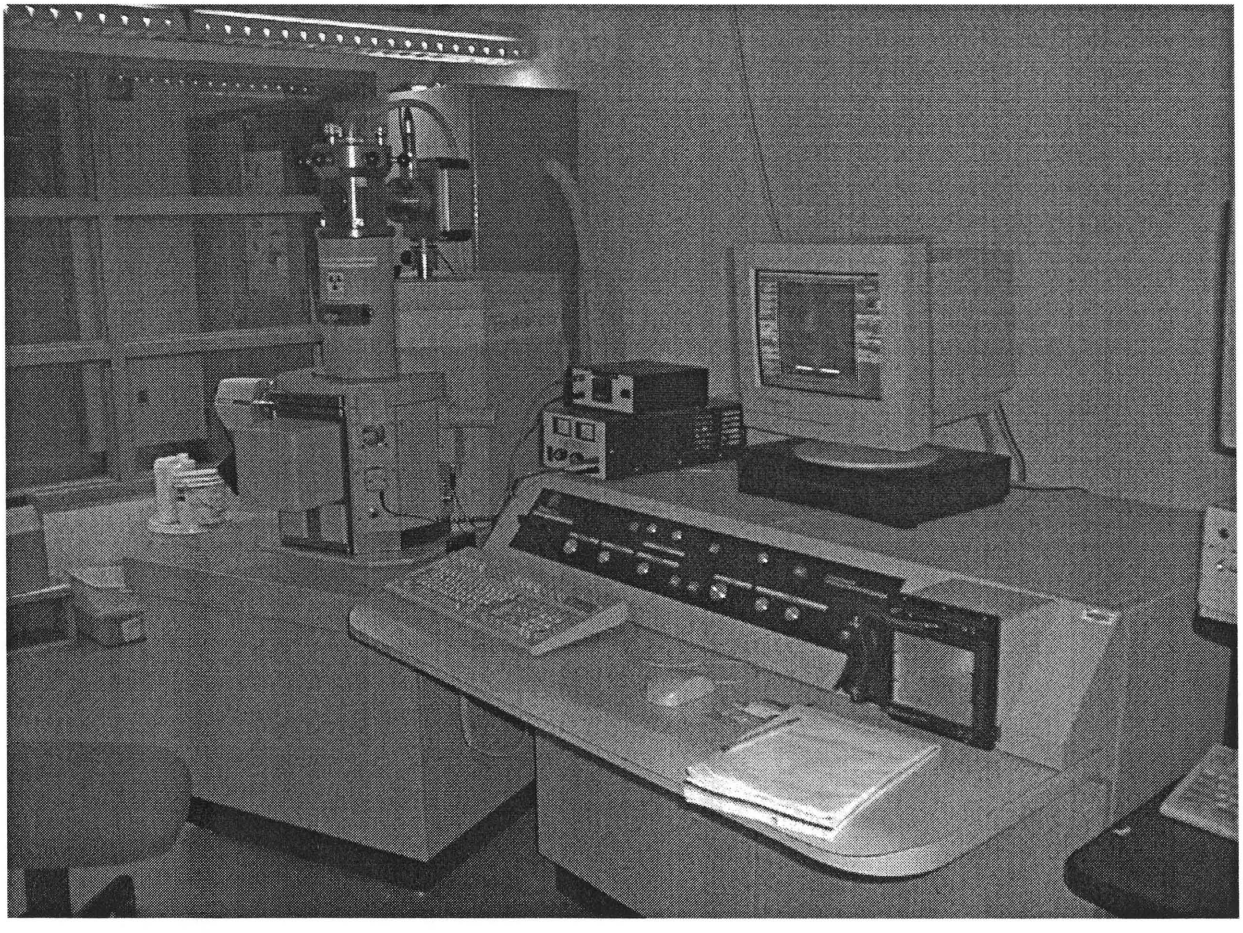

Figure 2.3 The Environmental Scanning Electron Microscope (ESEM)

The basic theory of ESEM is divided into three parts: Vacuum Basics, Detector Basics, and Gun Basics. In vacuum basics, the chamber pressure control is the main characteristic that shows the difference between the ESEM and the traditional SEM. The ESEM can operate in a wide range of pressure. Varying either chamber pressure or specimen temperature can control phase transitions. The significance processes, which have direct relation with the pressure in the chamber, are beam scattering, charge neutralization, and gaseous signal amplification. Beam scattering is desirable to decrease the path length of the incident beam. The scattered fraction of the beam creates an extended skirt around the unscattered fraction. The latter will contribute to a dc component to the imaging signal but carries no spatial information **[63]**. Beam scattering decreases with lower pressure and higher beam voltage.

The collision between moving electrons and neutral gas molecule will produce the density of free ions in the gas. At pressure greater than 1 Torr, the density is adequate to contribute a conductive path for beam-deposited surface charge yielding a smooth self-regulating equilibration of charge on insulating surfaces. However, at pressure above 5 Torr, this process always assume a stable equilibrium condition in response to changes in beam voltage, beam current, scanning speed, or surface characteristics.

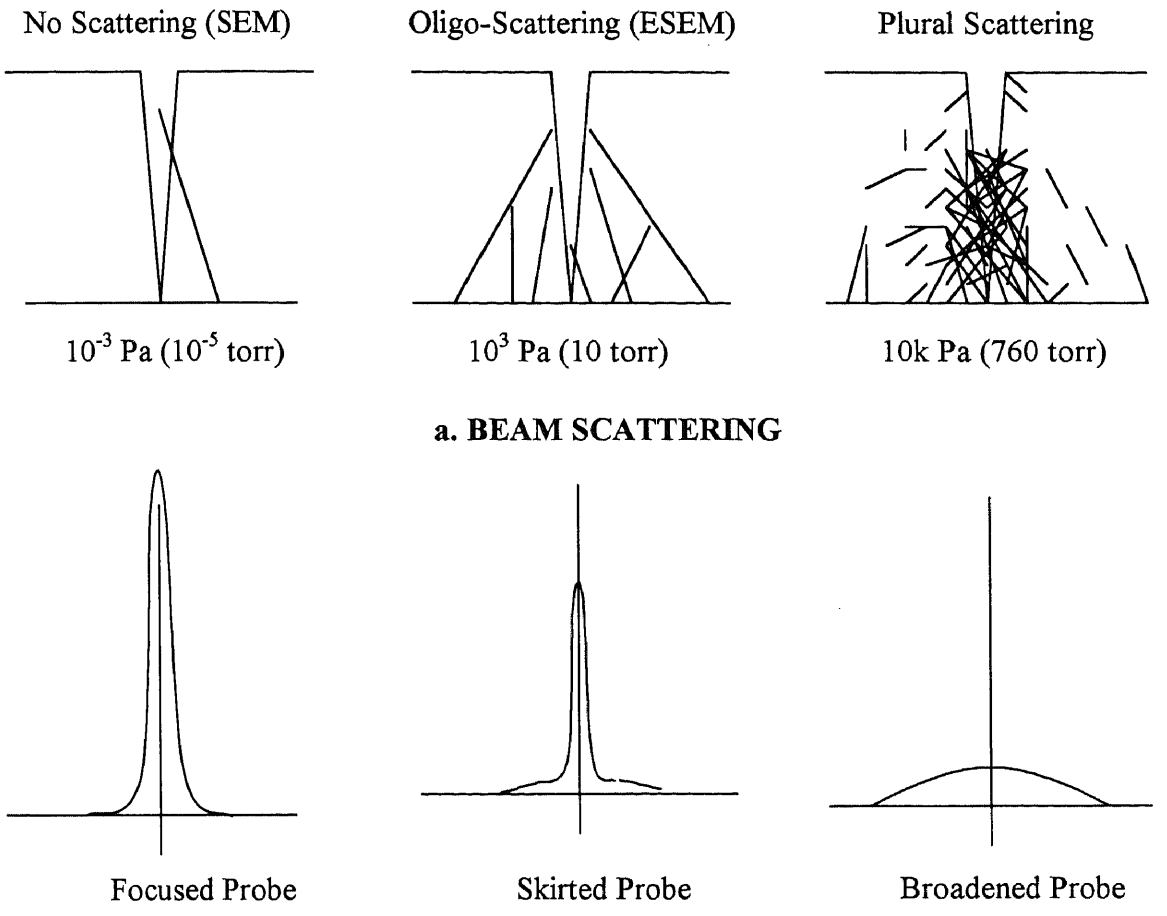

Figure 2.4 Beam Profiles as a Function of Pressure **[63]**.

The Gaseous Secondary Electron Detector (GSED) plays an important role in detector basics of the ESEM. The GSED utilizes gas ionization principles to collect and amplify the picoampere-level imaging signals generating from beam-specimen interaction. The gaseous detector contains one or more electrodes, which are united with the final pressure-limiting aperture. The action of charge between the electrode and the specimen holder generates a signal in the electronic circuit connected to the electrode.

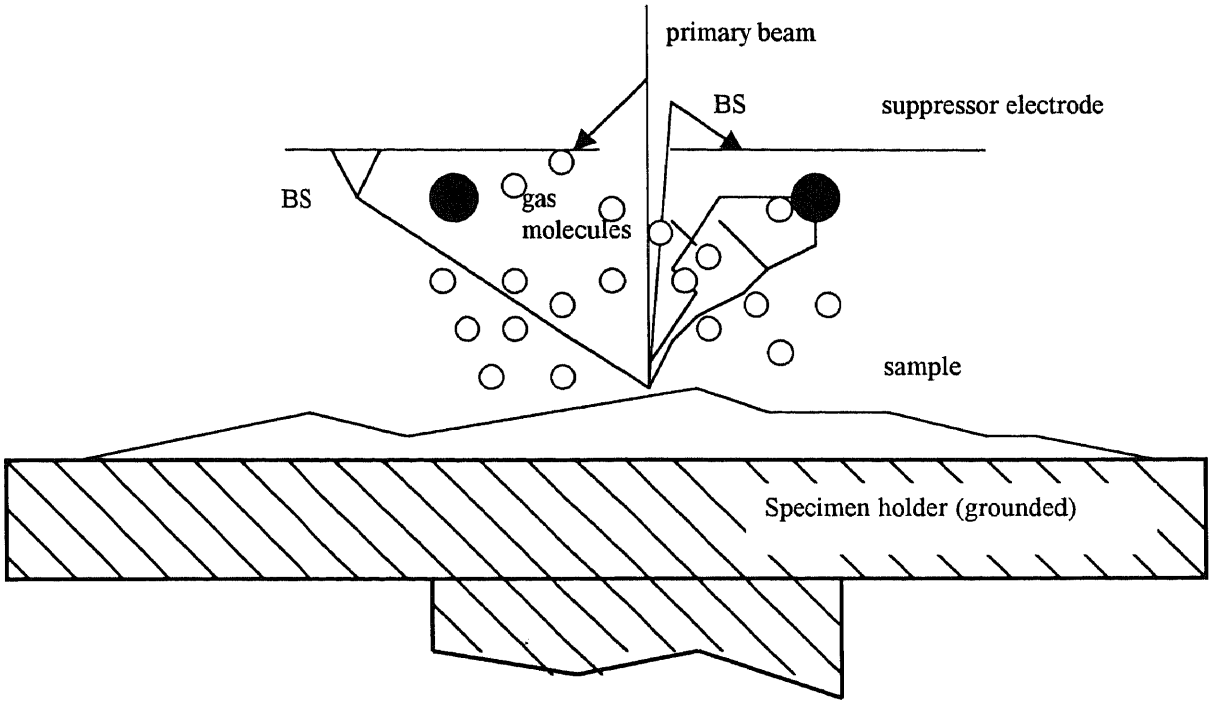

Figure 2.5 Signal Collection in the ESEM **[63]**.

Figure 2.5 illustrates the surface secondary electrons that emit from the sample are accelerated by the electric field until their velocity reach 20 eV the gas molecules will be ionized and produce more electrons. The efficiency of ionization is the function of pressure, working distance, and electrode voltage.

The free positive charge electrons are always brought about by ionization. The positives are gradually moved because of their large masses by the electric field in the opposite direction of cascaded electrons. These positives are not involved with imaging signal but carry out an important function by neutralizing surface buildup of electron charge.

Since the mean free path of high speed electrons is long, the collisions of backscatter electron flux from the specimen will not commonly occur in the detection volume. The pressure is the controlling factor for the relative proportions of secondary- and backscatter- initiated components in the imaging signal.

According to the interaction between focus beam of electron and the specimen, the information of sample material is obtained under the ESEM. An electron gun is used as a source of the electron beam. This gun consists of a heated cathode and other electrodes and performs at a high vacuum condition. An axially symmetric beam of electrons is extracted, controlled, and focused by the electron gun and then is demagnified and deflected by the optics in the lower column.

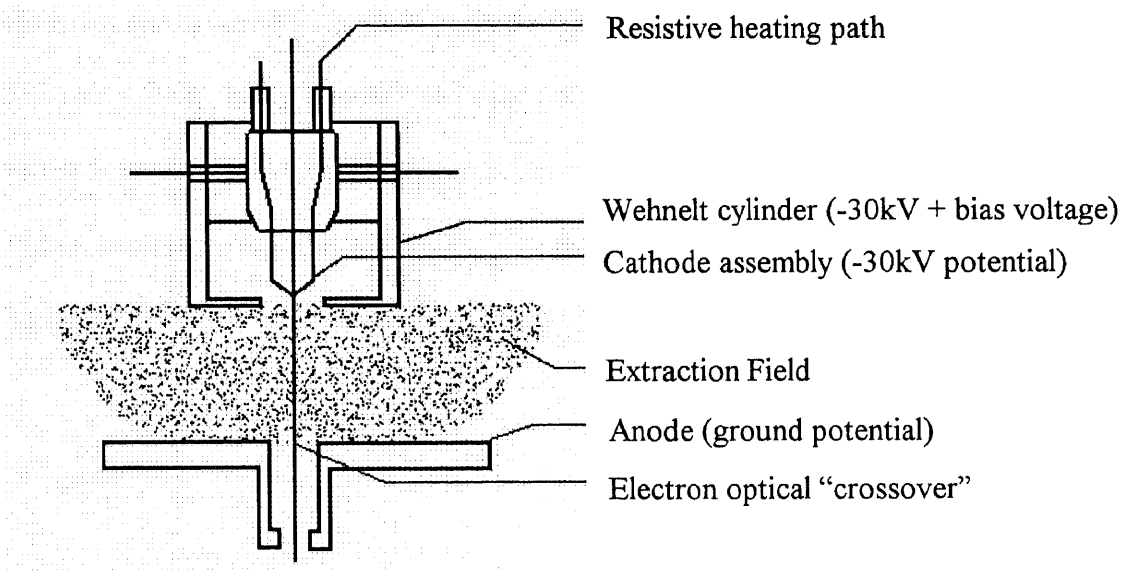

Figure 2.6 Basic Electron Gun **[63]**.

The cathode, a negatively-biased surface, resists to heat in a high vacuum circumstances. When heating the cathode, electrons will have enough energy to break through the surface barrier energy of the material. After that, electrons will be accelerated from the potential of the gun headed for the more positive potential of the anode.

The emission current, the free electrons flow, is arranged by the stable heating current of cathode and becomes important by the action of the bias voltage, a repulsive field from the Wehnelt cylinder. The application of bias voltage has a tendency to decrease the emission current by limiting the electron emitting area on the cathode surface. The higher the temperature of the cathode and the more restricted the emitting surface area, the brighter the electron source will be.

Lanthanum hexaboride (LaB_6) had been used as a cathode in this study. The electrons discharged from a LaB_6 cathode are greater than those from a tungsten cathode because a LaB_6 has a smaller emitting area than tungsten. When more electrons are focused down to strike the sample, a brighter image is given. Hence, it contributes better resolution under high magnification. The disadvantages of using the LaB_6 cathode are high cost and extra care requirements when operating the equipment.

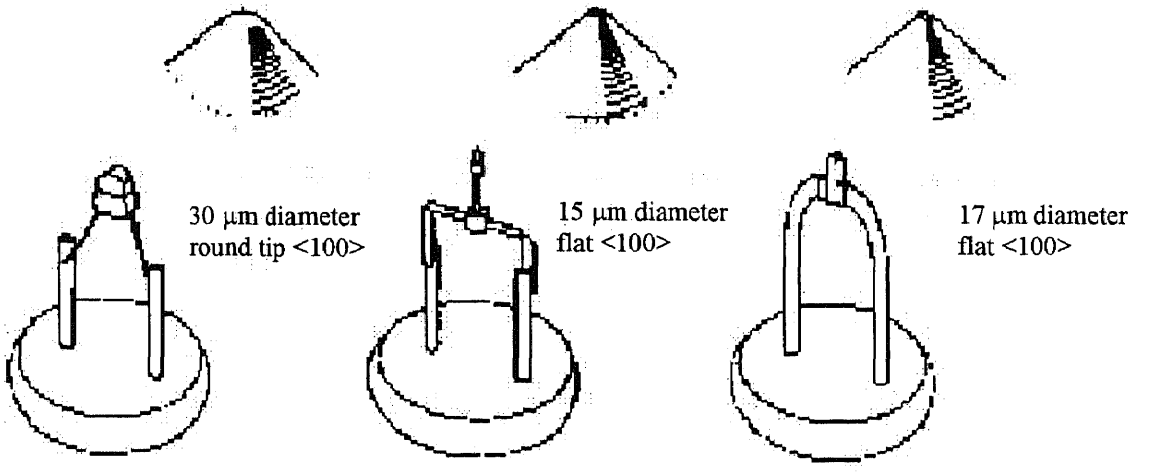

(a) Denka M-3 (b) Kimball Physics ES-423E (c) FEI Corp. Mini Vogel Mount

Figure 2.7 Different Types of LaB_6 Cathodes **[63]**.

Procedure followed for sample observation using ESEM:

1. The computer and column console of the ESEM are first turned on to ramp the filament to an operating current of 2.25A and bringing up the operating beam voltage to 20kv and maintain a pressure of 5.0Torr in the specimen chamber.
2. The sample to be observed is adhered to a specimen holder by using a conductive carbon paste and inserted into the specimen chamber by first bringing up the pressure in the specimen chamber to 100 Torr.
3. Once the sample is inserted the chamber door is closed and once again the pressure lowered to an operating pressure of 5 Torr. The chamber is then flooded with water vapor as it is a good imaging gas and it remove traces of air.

4. The stage on which the sample rests can move in the X, Y and Z axis. These parameters are adjusted to bring the sample closer to the detector tip. Then the contrast, and brightness and focus, condenser current etc are manually adjusted to obtain the best possible image for the required magnification.

2.4 Experiment

A synthetic sample was first prepared and measured the basic characteristic such as turbidity. Flocculation was carried out by using the jar test procedure. The lowest turbidity was achieved with a Fe^{+3} concentration of 10 mg/l and a cationic polyelectrolyte concentration of 4 mg/l. As a result of this jar test study, all the flocculation experiments were conducted with this Fe^{+3} concentration and polyelectrolyte concentration. Take the sample floc out and let it dry at room temperature. The floc is then investigate by using the Environmental Scanning Electron Microscope (ESEM).

The basic operating conditions for a jar test such as rapid mixing rate and duration, flocculation mixing rate and duration, size and type of microcarrier etc. are adopted from a process developed by Dr. Yuan Ding **[33]**.

CHAPTER 3

RESULTS AND DISCUSSION

This chapter discusses the experimental results from 2 stages of the experiment: the prescreening test and observation under the ESEM. The prescreening test was done in order to determine the optimal dosages of electrolyte and polyelectrolyte in the weighted flocculation process. The ESEM was employed to investigate the structure of the flocs from weighted flocculation.

3.1 Prescreening Test

In the prescreening test, flocculation was carried out by the jar test procedure. A known amount of microcarrier, various concentrations of electrolyte and polyelectrolyte were used. The turbidity of the raw sample was measured before performing the tests. It was 44.0 NTU. In the rapid mixing stage, a rate of 150 rpm for 10 seconds was required to lift microcarriers from the bottom of the jar into suspension. When the mixing rate was reduced to 100 rpm for 20 seconds, the beginning of floc growth was observed. During flocculation mixing, it was observed that flocs grow gradually and both microcarriers and flocs would settle within 30 seconds after the process completed. The supernatants were taken after 3 minutes settling time. Then the solutions were analyzed for turbidity. On the basis of turbidity, the optimal dosages of electrolyte and polyelectrolyte were achieved. Table 3-1, 3-2, and 3-3 show the experimental conditions, the remaining turbidity after flocculation, and the percent turbidity removal at different concentrations of electrolyte and polyelectrolyte.

Table 3.1 Observation at the Concentration of Fe^{+3} 10 mg/L

PARAMETER	Jar 1	Jar 2	Jar 3	Jar 4	Jar 5	Jar 6	Jar 7
Microcarrier Type	Ottawa Sand						
Microcarrier Size	53-75 micrometer						
Microcarrier Concentration	3 gm.						
Settling Time	3 minutes						
Fe^{+3} Concentration (mg/L)	10						
309C Concentration (mg/L)	0	1	2	3	4	5	6
Turbidity	154.00	2.87	0.62	0.22	0.16	0.19	0.17
% Turbidity Removal	0	93.48	98.59	99.50	99.64	99.57	99.61

Table 3.2 Observation at the concentration of Fe^{+3} 20 mg/L

PARAMETER	Jar 1	Jar 2	Jar 3	Jar 4	Jar 5	Jar 6	Jar 7
Microcarrier Type	Ottawa Sand						
Microcarrier Size	53-75 micrometer						
Microcarrier Concentration	3 gm.						
Settling Time	3 minutes						
Fe^{+3} Concentration (mg/L)	20						
309C Concentration (mg/L)	0	1	2	3	4	5	6
Turbidity	48.00	1.20	0.52	0.35	0.28	0.30	0.51
% Turbidity Removal	0	97.27	98.82	99.20	99.36	99.32	98.84

Table 3.3 Observation at the concentration of Fe^{+3} 30 mg/L

PARAMETER	Jar 1	Jar 2	Jar 3	Jar 4	Jar 5	Jar 6	Jar 7
Microcarrier Type	Ottawa Sand						
Microcarrier Size	53-75 micrometer						
Microcarrier Concentration	3 gm.						
Settling Time	3 minutes						
Fe^{+3} Concentration (mg/L)	30						
309C Concentration (mg/L)	0	1	2	3	4	5	6
Turbidity	126.00	1.87	0.63	0.40	0.30	0.33	0.53
% Turbidity Removal	0	95.75	98.57	99.09	99.32	99.25	98.80

From Table 3.1, 3.2, and 3.3, the results show that in the absence of polyelectrolyte in the solution, the residual turbidity increased appreciably. On the other hand, with the additional of polyelectrolyte, the turbidity removals fall in the range of 93.48% to 99.64%.

Figure 3.1, 3.2, and 3.3 illustrate the turbidity distribution versus polyelectrolyte concentration for the Fe^{+3} concentration of 10 mg/L, 20 mg/L, and 30 mg/L, respectively. It can be seen that the lowest remaining turbidities for all Fe^{+3} concentrations are at 4 mg/L of the 309C concentration.

Figure 3.4 illustrates the turbidity of raw sample, 44.00 NTU, compared to the lowest remaining turbidity of each electrolyte concentration, 0.16 NTU at 10 mg/L of Fe^{+3}, 0.28 NTU at 20 mg/L of Fe^{+3}, and 0.30 NTU at 30 mg/L of Fe^{+3}. The best electrolyte concentration is the one that has the lowest remaining turbidity, which is at 10

mg/L. The turbidity removal was about 99.64%. The 10 mg/L of Fe^{+3} and 4 mg/L of 309C can be considered as the optimal coagulant concentrations. They had been chosen to conduct all the tests.

According to the experimental results of Dr. Yuan Ding **[33]** for the combined sewer overflows (CSO) treatment, the utilization of microcarrier in a size range of 53 to 75 micrometers at a dosage of 3 g/L, Fe^{+3} concentration of 40 mg/L, 309C concentration of 6 mg/L, and settling time of 3 minutes was found to yield the best turbidity removal. The turbidity was removed about 98%. Figure 3.5 compares the turbidity of CSO sample between raw sample and after treatment.

It can be concluded that the effectiveness of weighted flocculation in the synthetic sample treatment is as well as in the CSO treatment on the turbidity basis.

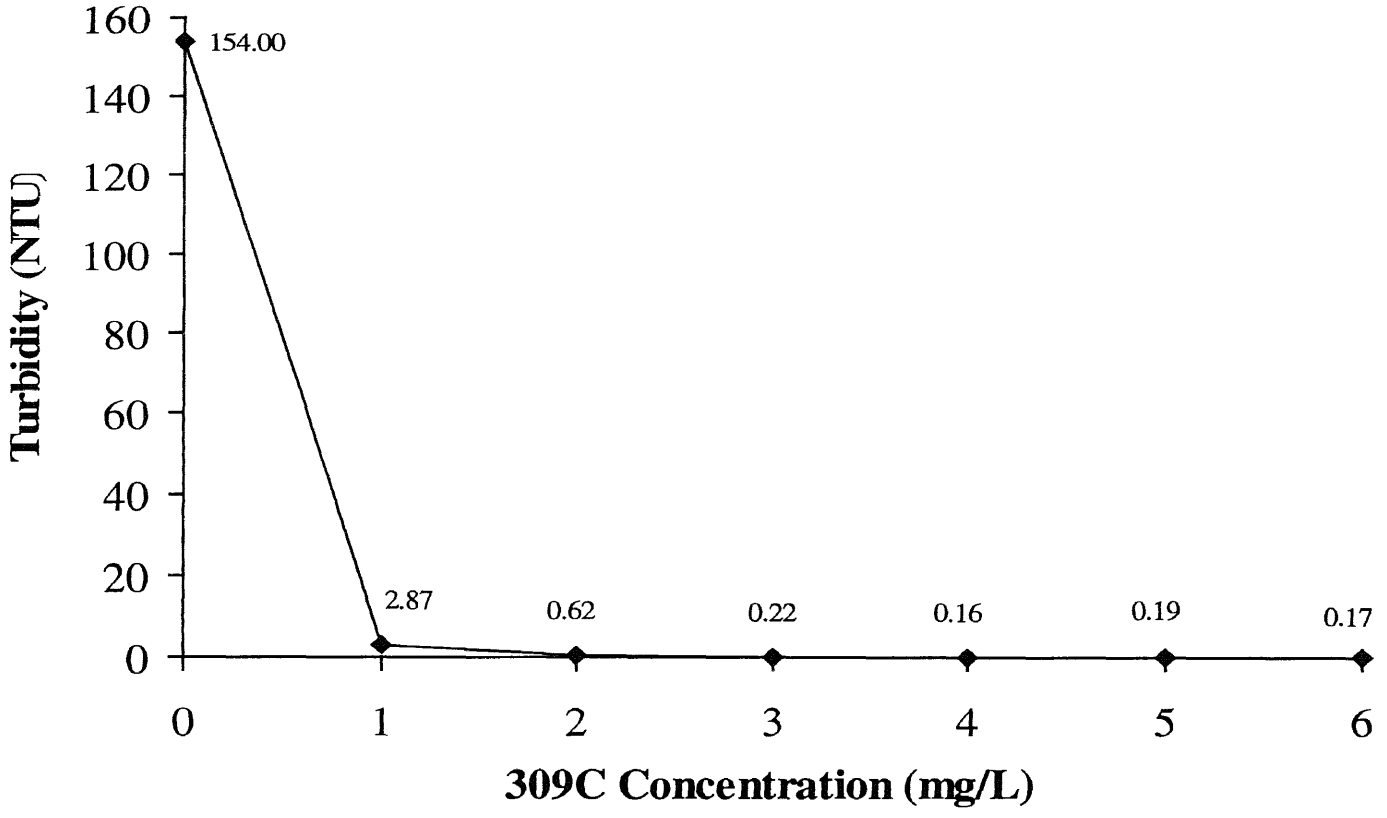

Figure 3.1 Turbidity Versus Polyelectrolyte Concentration for 10 mg/L of Fe^{+3}.

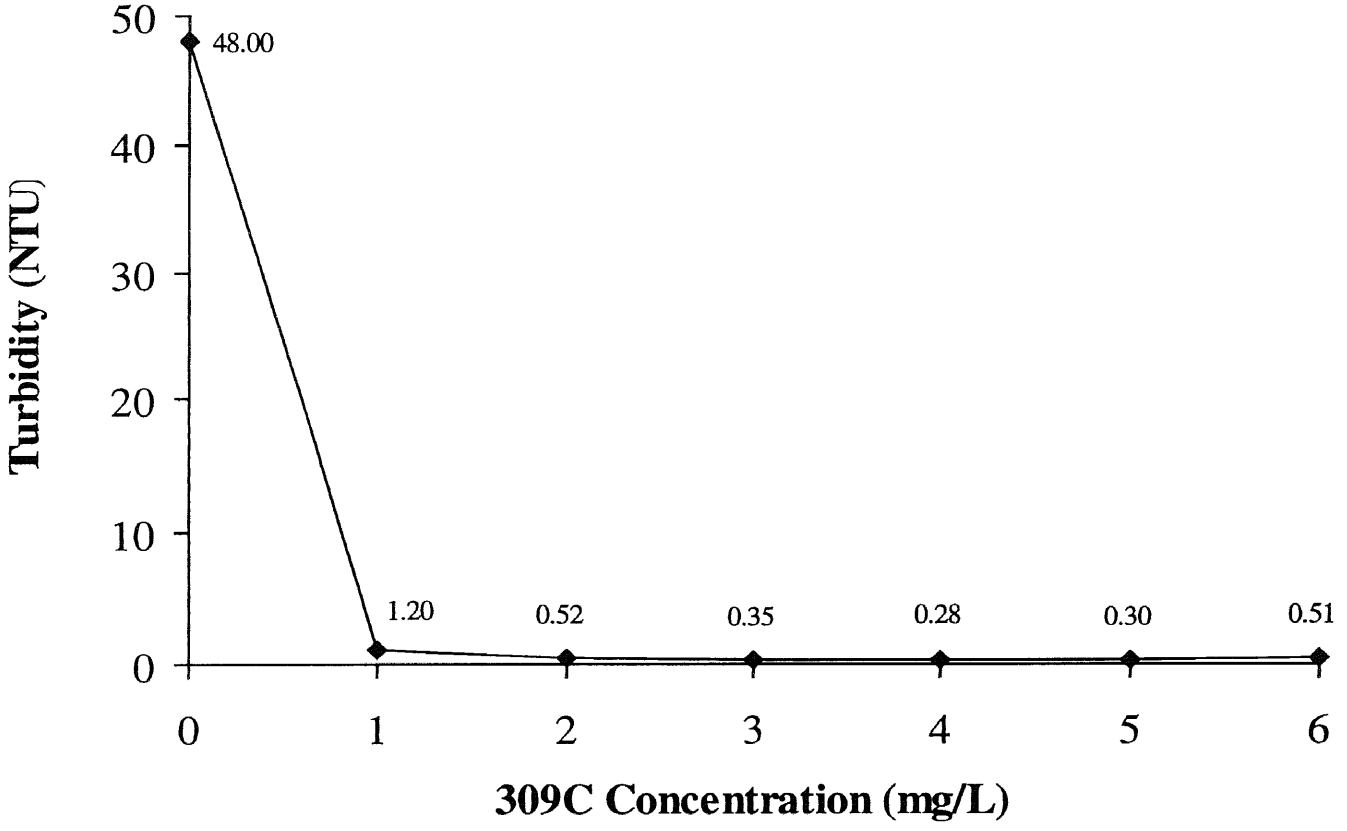

Figure 3.2 Turbidity Versus Polyelectrolyte Concentration for 20 mg/L of Fe^{+3}.

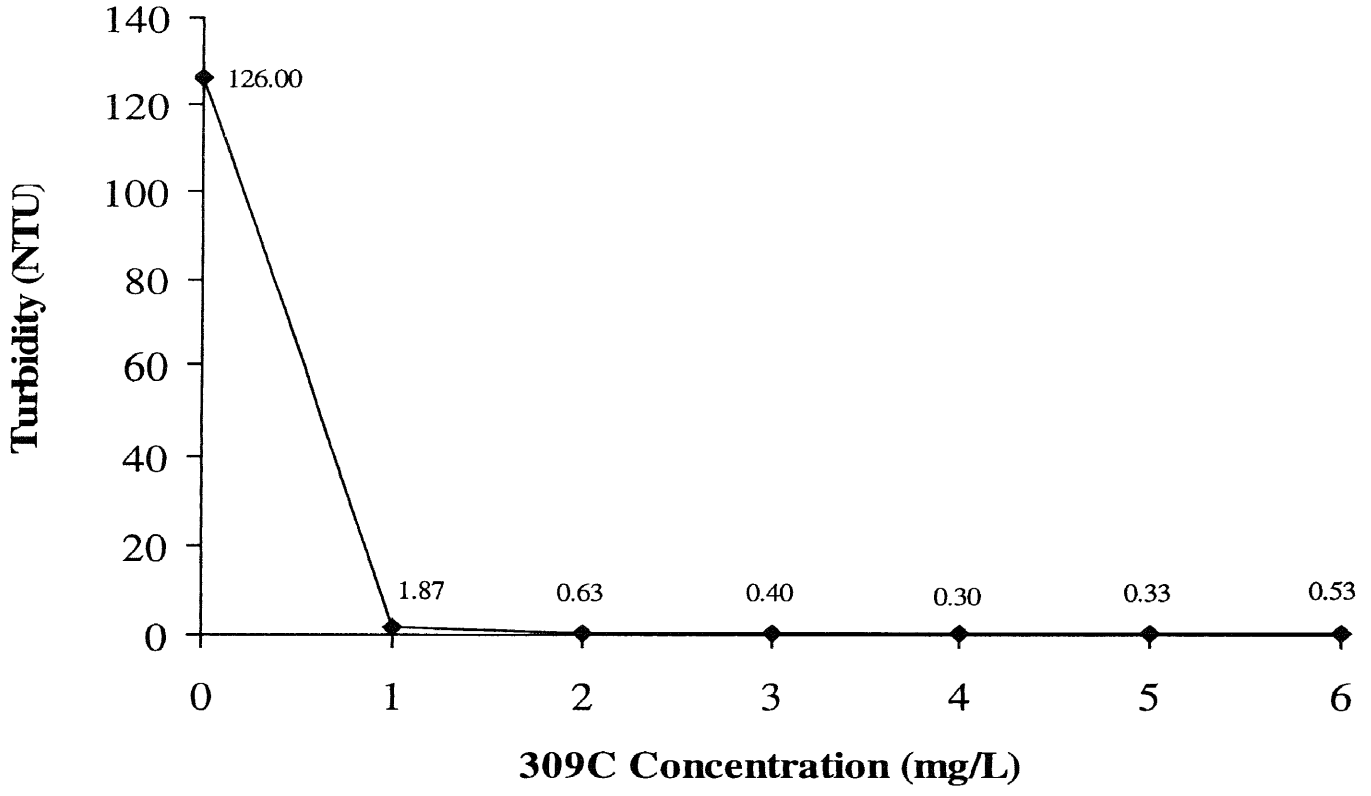

Figure 3.3 Turbidity Versus Polyelectrolyte Concentration for 30 mg/L of Fe^{+3}.

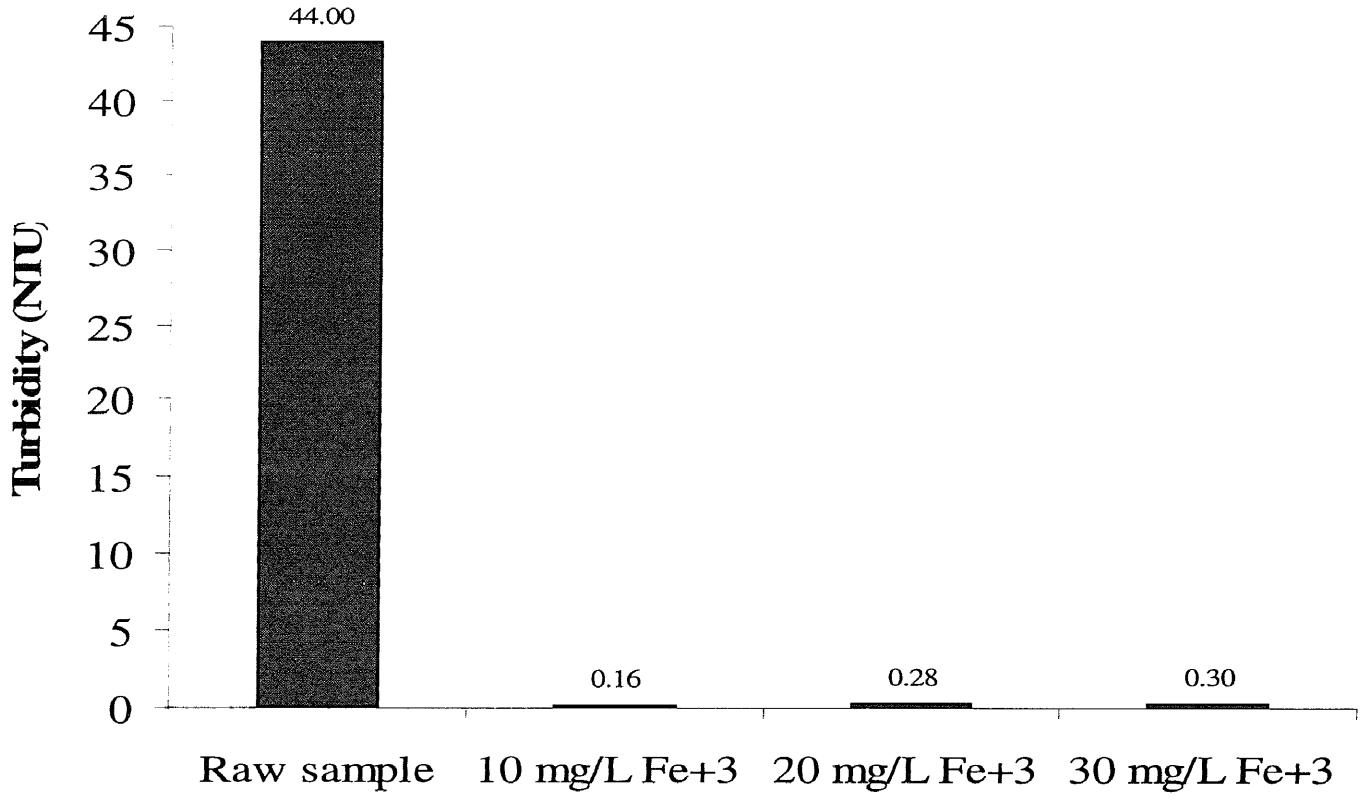

Figure 3.4 Effectiveness of the Weighted Flocculation Process.

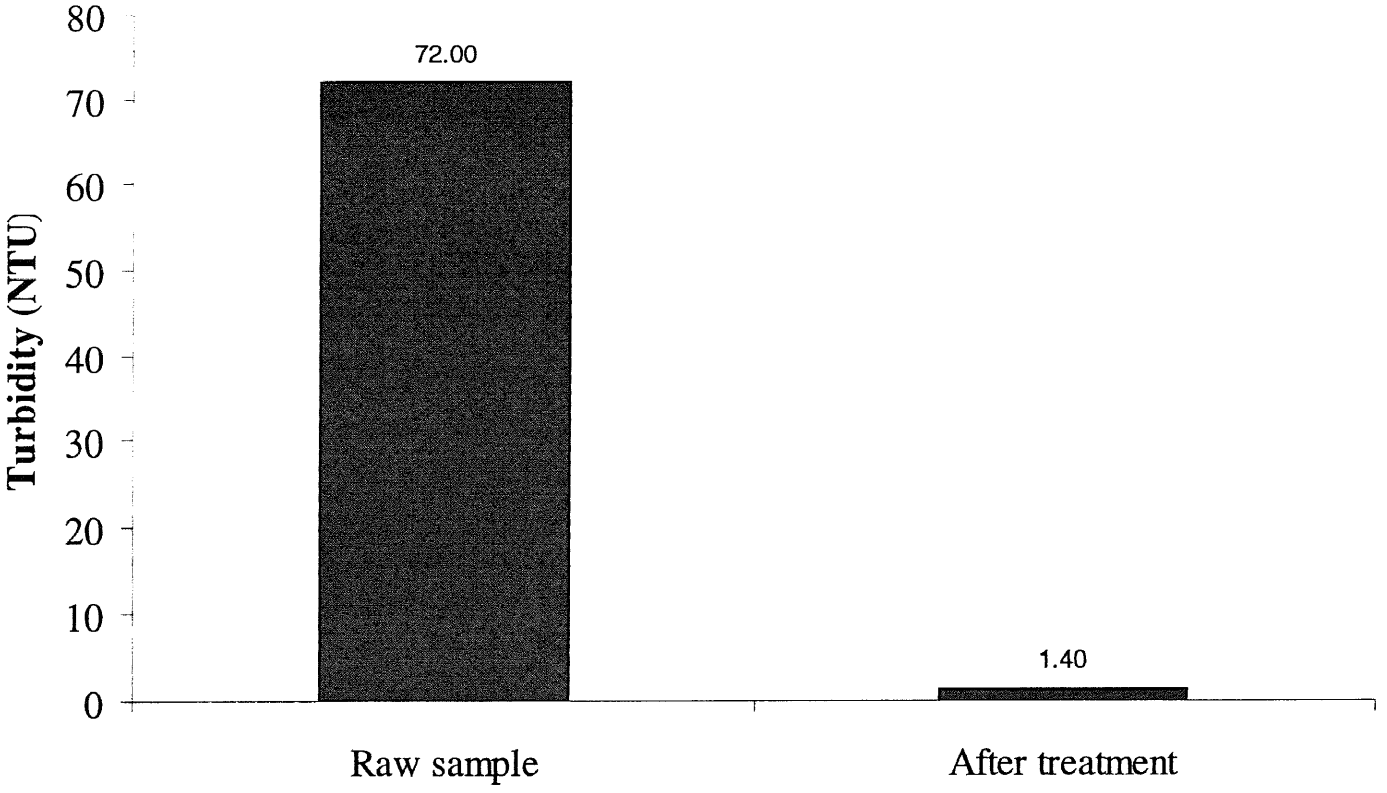

Figure 3.5 Effectiveness of the Weighted Flocculation Process in CSO Treatment.

3.2 Observation Results from the ESEM

3.2.1 Microcarrier

After grinding, sieving, washing, and drying the microcarriers, it was observed under the ESEM that they are not spherical in shape but amorphous as shown in Figure 3.6. Most of the surface areas are clear and smooth. They are also different in size. Although the size of microcarrier used in the experiments were in the range of 53 to 75 micrometers, some of the microcarriers were greater than 75 micrometers. Figure 3.6 also shows that the length of some microcarriers falls in the range of 53 to 75 micrometers. As a result, they could pass the sieve. This picture was obtained under the conditions of 3.7 Torr of pressure, 20.5 mm of the focus length, and magnification of 380x.

Figure 3.7 was completed under the conditions of 3.8 Torr of pressure, 20.6 mm of the focus length, and magnification of 2000x. It shows the closer view of the microcarrier surface. There is nothing attaching to their surfaces and edges.

3.2.2 Dry Sample

The dry sample was collected from NJIT parking lot #6. These samples were sieved, washed, and dried. Figure 3.8 presents the overview of dry sample. They were observed that their shapes are amorphous. The surface is not smooth. They are different in size. This investigation was done under the conditions of 5.0 Torr of pressure, 18.6 mm of the focus length, and magnification of 300x.

Figure 3.9 was acquired under the conditions of 5.2 Torr of pressure, 18.7 mm of the focus length, and magnification of 900x. It can be seen that there are a lot of small particles attached to its surface.

3.2.3 Weighted Flocs

These flocs were taken after settling for 3 minutes and dried at room temperature. Figure 3.10 displays that the surface of the microcarrier is not clean and smooth but there are some small particles sticking on and coating it. This examination was performed under the conditions of 5.2 Torr of pressure, 18.9 mm of the focus length, and magnification of 850x.

Figure 3.11 reveals the closer view of the previous figure showing that there are some substances coating the surface compared to the picture of microcarrier in Figure 3.6. This picture was accomplished under the conditions of 5.1 Torr of pressure, 18.9 mm of the focus length, and magnification of 4950x.

From the figure 3.12 and 3.13, there are some vacant spaces on the surfaces of microcarriers for sample to stick on. It can be presumed to increase the efficiency of the process by increasing the concentration of sample into the process. Figure 3.12 and 3.13 were accomplished under the conditions of 5.2 Torr of pressure, 19.6 mm of the focus length, and magnification of 500x.

It can be seen that microcarrier does play a significant role in the removal of colloidal particles. On conducting the tests, colloidal particles attached to microcarriers with the presence of electrolyte and polyelectrolyte in the solutions. These coagulants initiate charge neutralization and polymer bridging that play an important role in the destabilization of colloidal particles.

Some experimental studies had shown that partially structural information of flocs might lose during the drying process. The sample preparation of ESEM analysis involves evacuation of moisture under high vacuum, therefore it might change the arrangement of

the particles in the aggregates and its structure. The freeze fracture technique is recommended by some researchers to use in order to ensure that the floc structure is not altered to a notable extent during a stage of sample preparation.

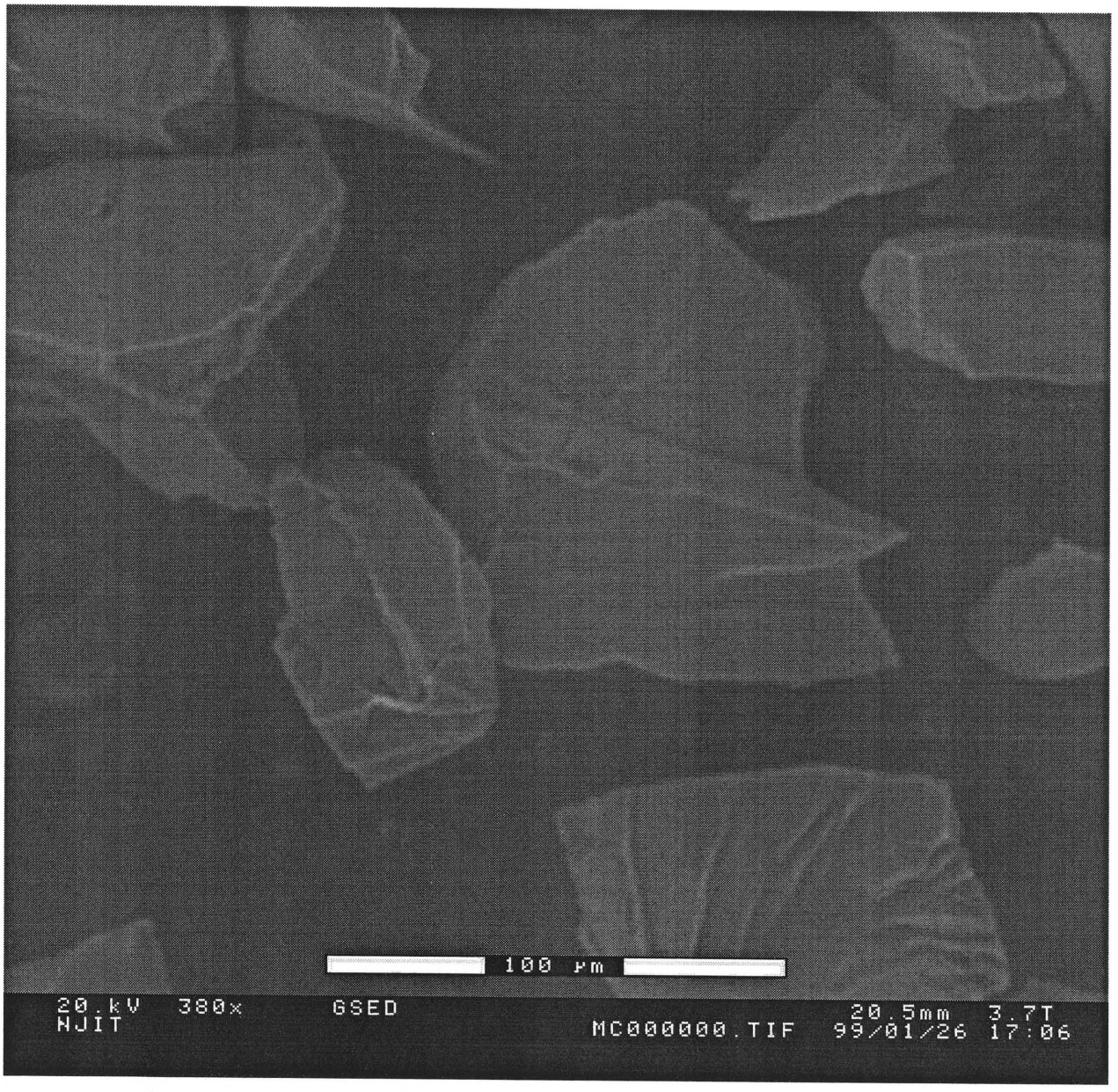

Figure 3.6 Microcarrier Obtained Under Magnification of 380x.

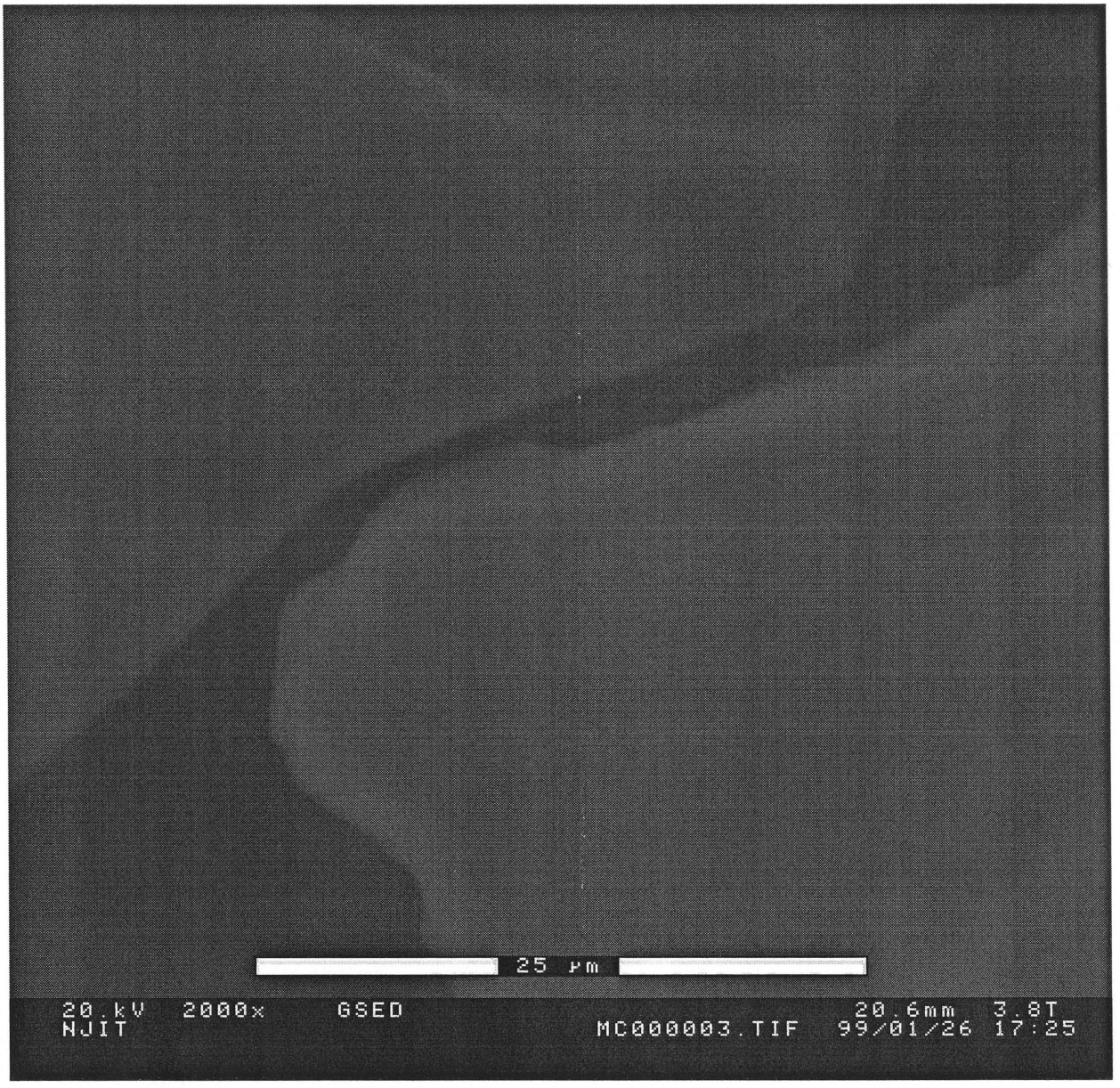

Figure 3.7 Microcarrier Obtained Under Magnification of 2000x.

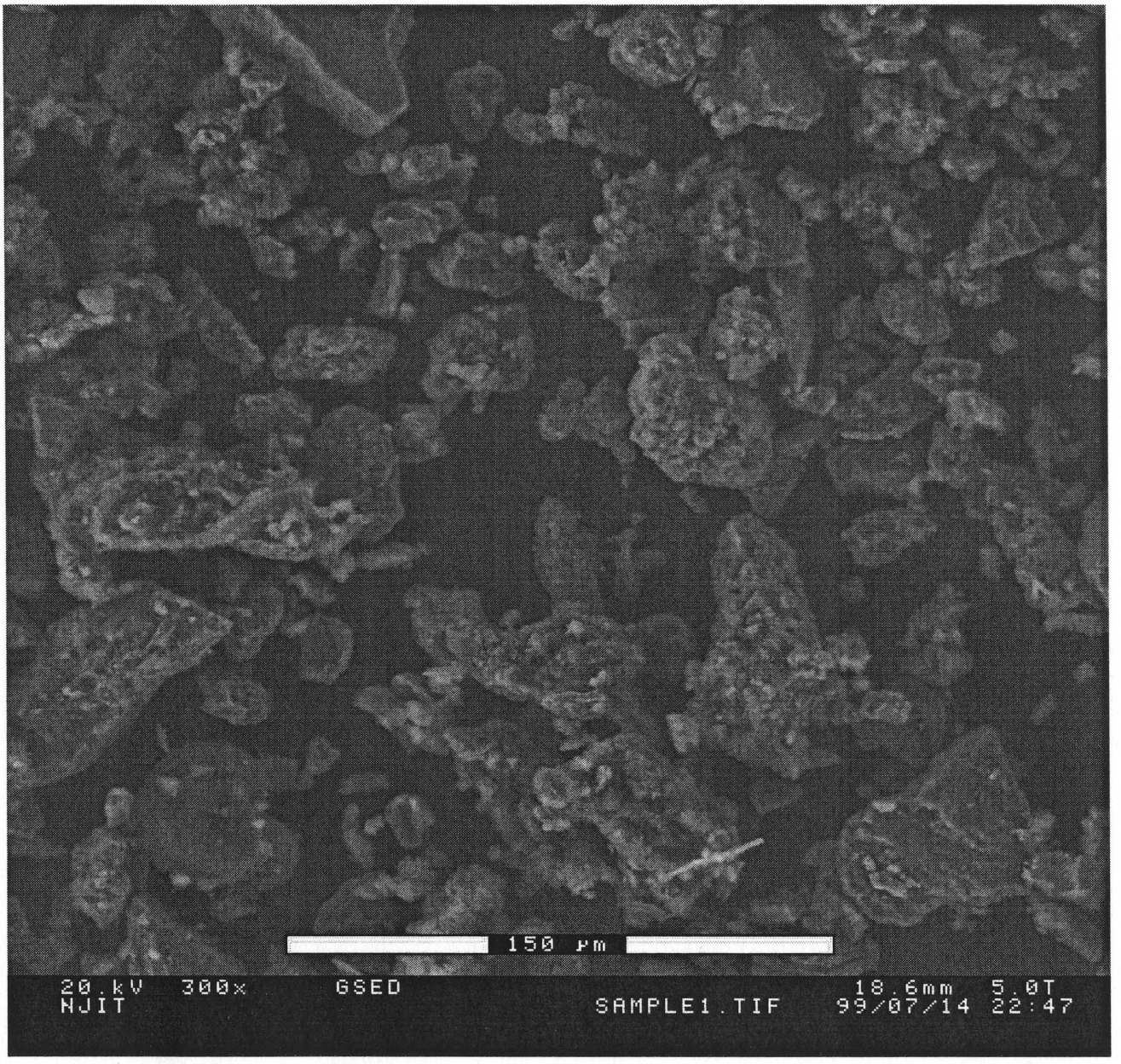

Figure 3.8 Dry Sample Obtained Under Magnification of 300x

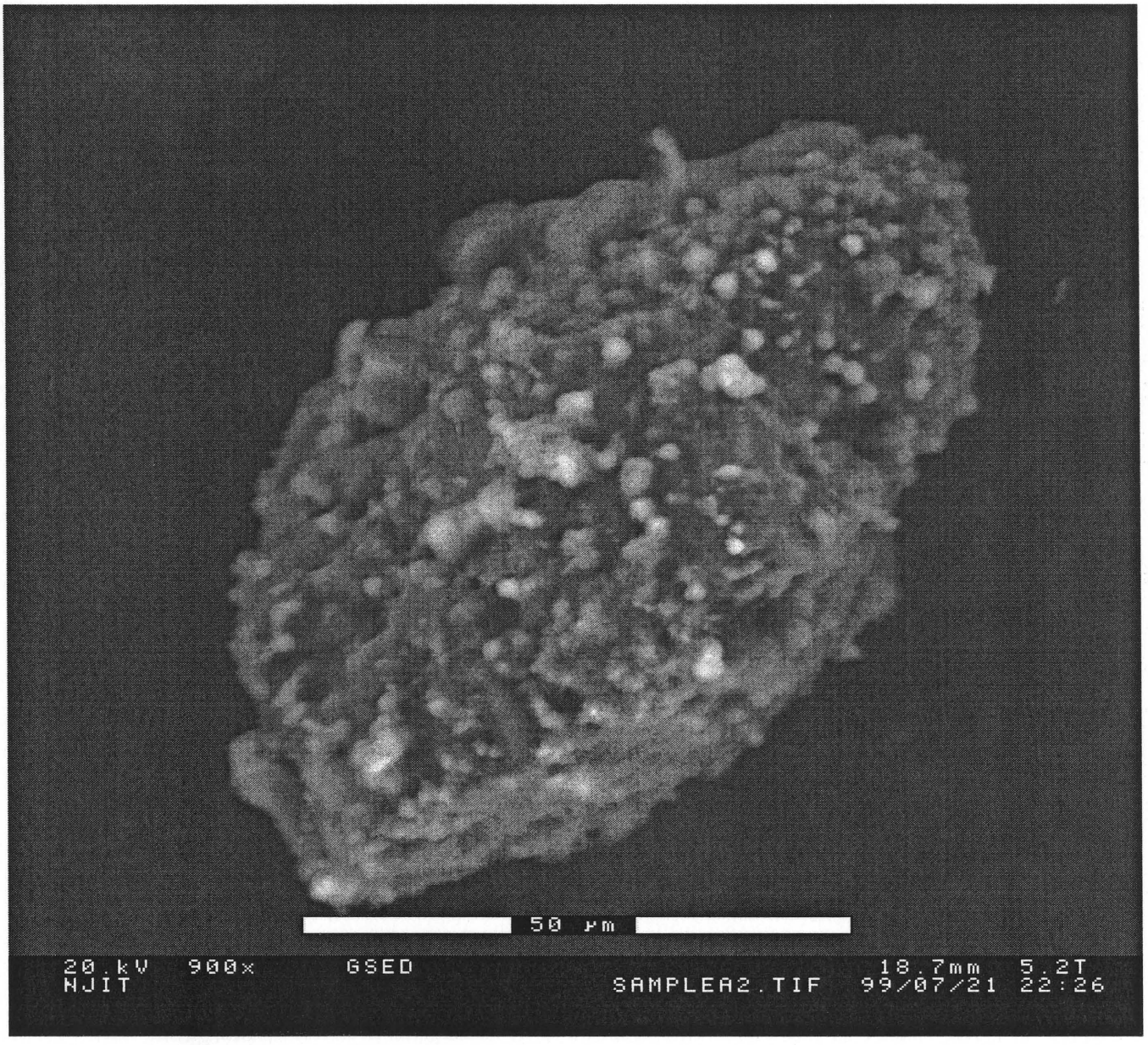

Figure 3.9 Dry Sample Obtained Under Magnification of 900x.

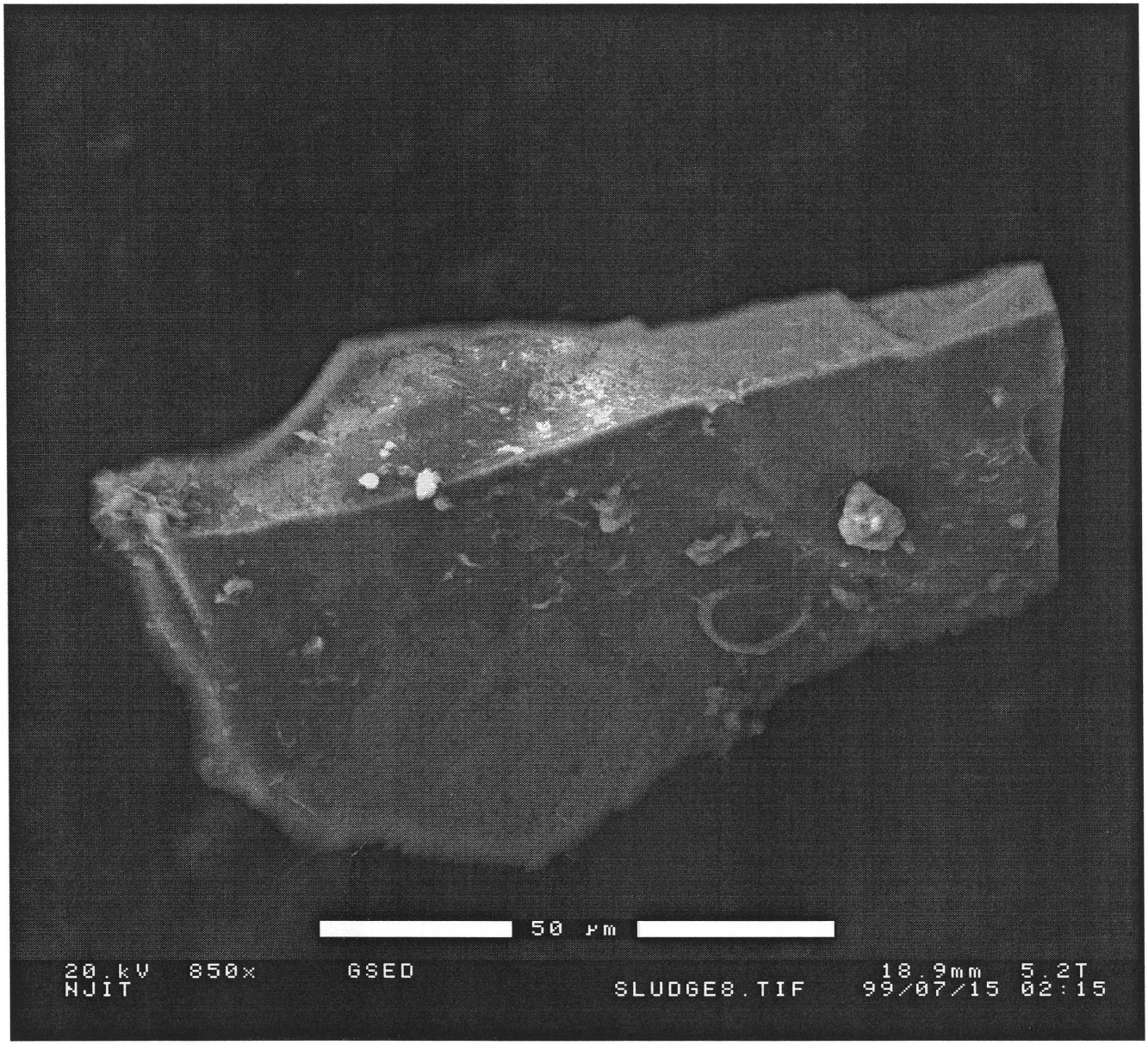

Figure 3.10 Weighted Floc Obtained Under Magnification of 850x.

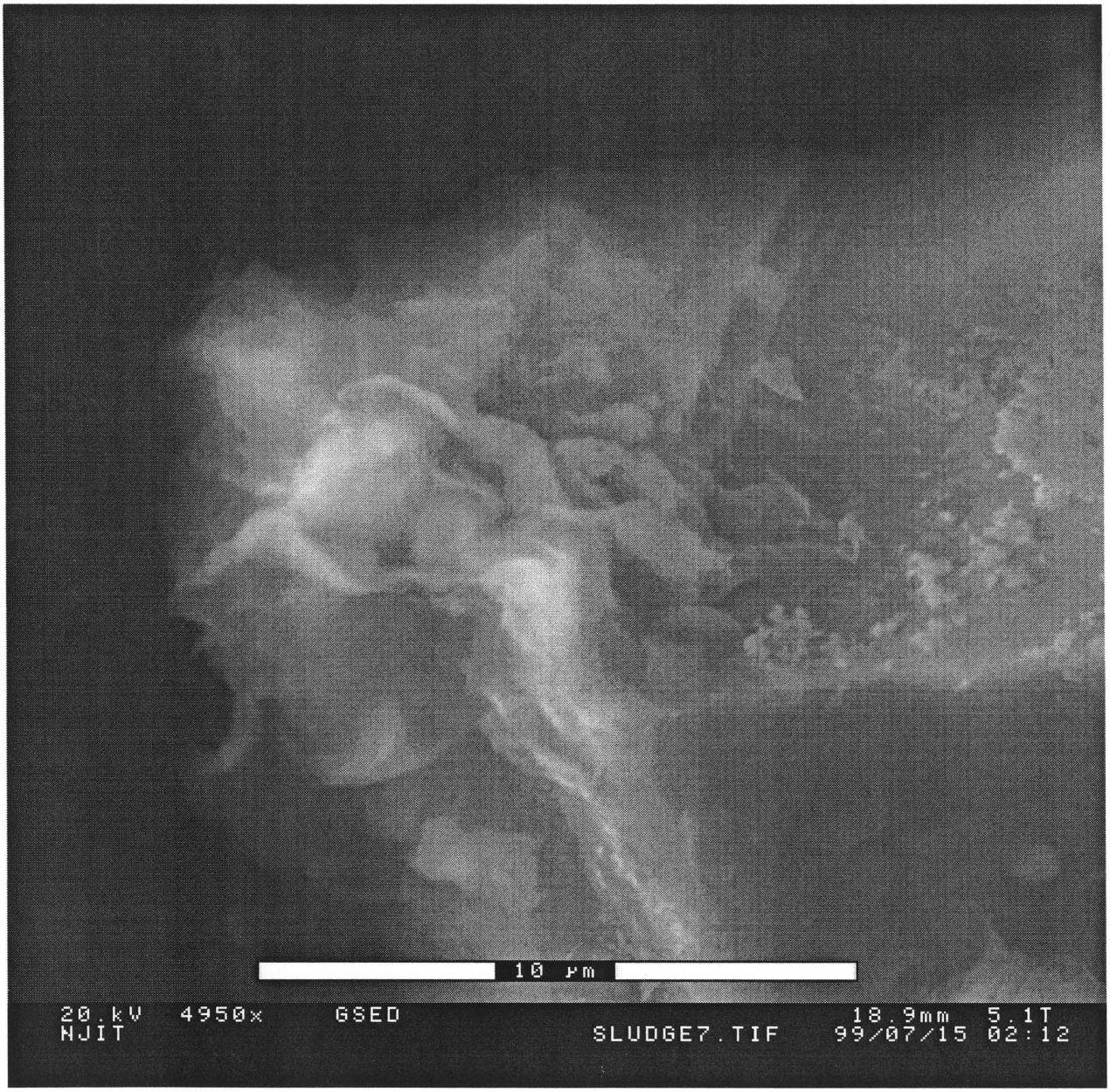

Figure 3.11 Weighted Floc Obtained Under Magnification of 4950x.

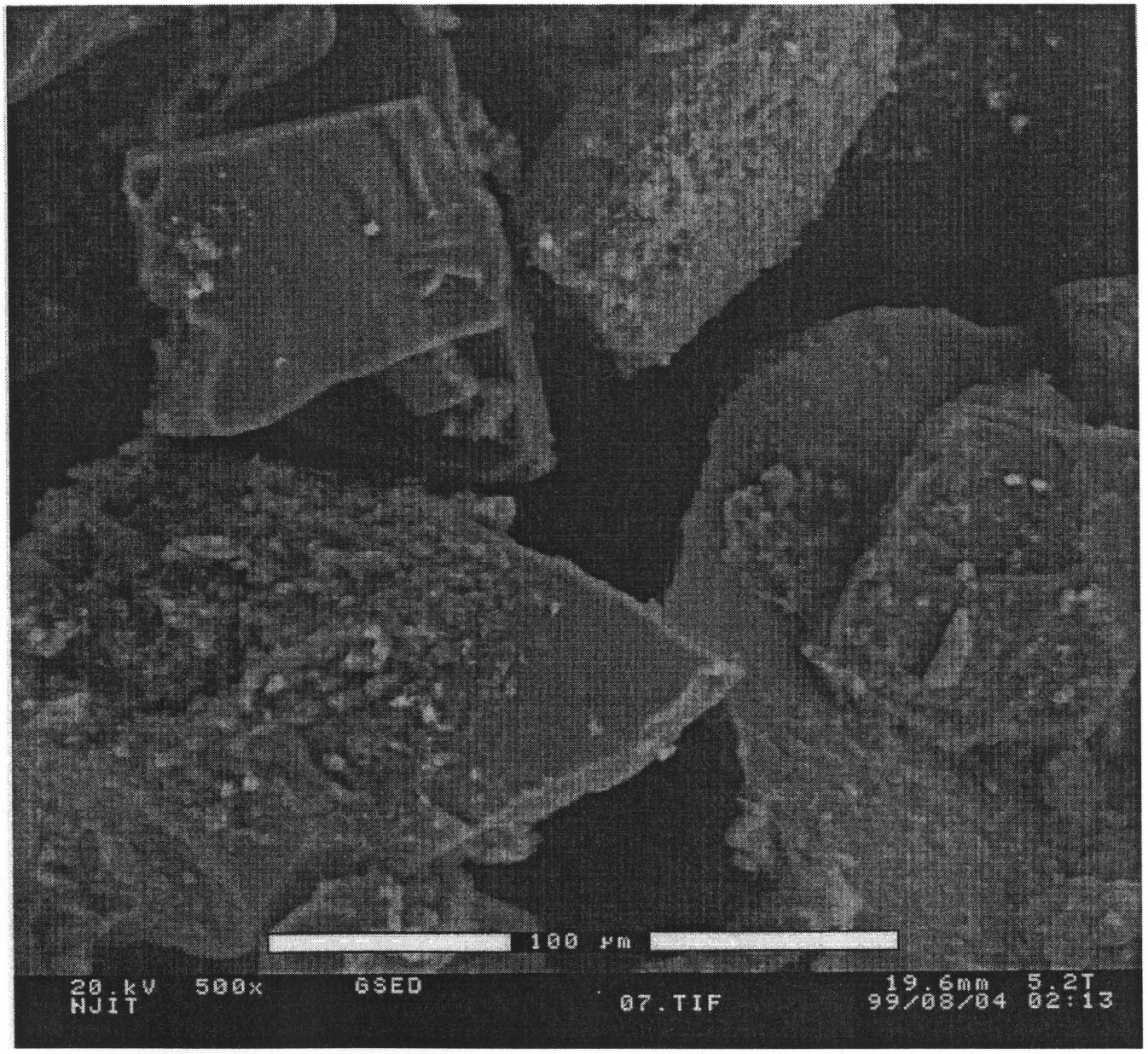

Figure 3.12 Weighted Floc Obtained Under Magnification of 500x (1).

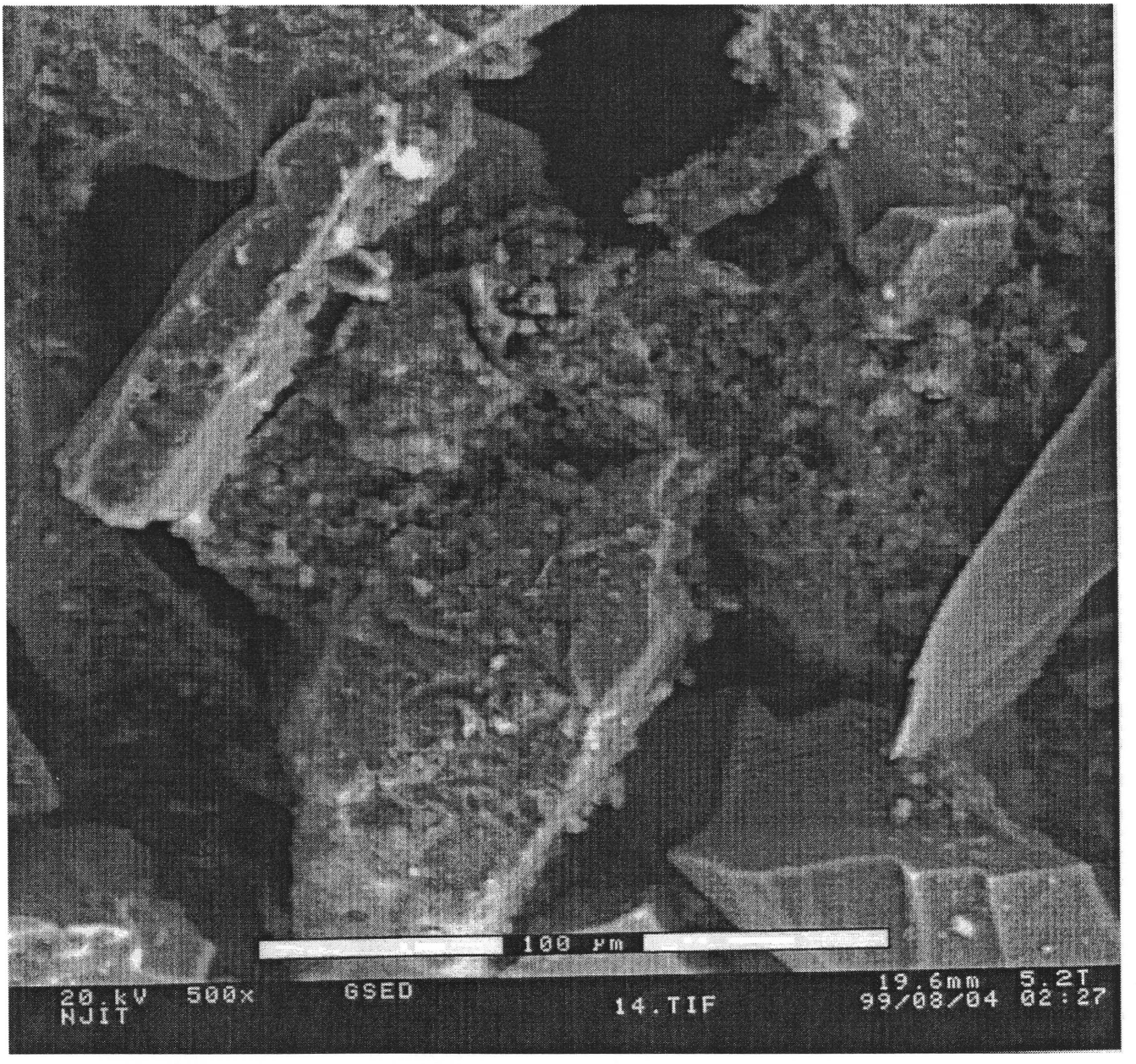

Figure 3.13 Weighted Floc Obtained Under Magnification of 500x (2).

CHAPTER 4

CONCLUSIONS AND RECOMMENDATIONS

4.1 Conclusions

On the basis of the results of this study, the principal conclusions can be summarized as follows:

1. Microcarrier did play a significant role in the removal of colloidal particles. Electrolyte and polyelectrolyte needed to add into the process in order to induce the charge neutralization and polymer bridging process.
2. In the presence of electrolyte and polyelectrolyte, the turbidity removal fell in the range of 93.5% to 99.6%, while the removal turbidity in CSO treatment was about 98%. As a result, the effectiveness in turbidity removal of the weighted flocculation process for synthetic sample treatment was as well as that of for CSO treatment.
3. The observations under the ESEM showed that the microcarrier was amorphous and different in size. The surfaces were smooth and clear.
4. For the dry sample, the photographs showed that they were also amorphous and consisted of a lot of colloidal particles.
5. It was clear that the flocs from weighted flocculation consisted of a population of amorphous particles.

4.2 Recommendations

To further study in this area, the following investigations are recommended:

1. Elemental analysis should be performed in order to identify the elements in the floc.
2. To minimize the destruction of floc structure that might occur during the drying process and to achieve a good image of floc structure, the freeze fracture technique should be employed.
3. The ESEM observations using a drying process might not be suitable for weighted floc. Therefore other techniques such as the light scattering, Transmission Electron Microscopy (TEM), etc., which do not need to dry sample, should be employed.

REFERENCES

1) J. Gregory, "The Role of Colloid Interactions in Solid-Liquid Separation," *Wat. Sci. Tech.*, Vol. 27, No. 10, pp. 1-17, 1993.

2) J. Gregory, "Approximate Expressions for retarded van der Waals interaction," *J. Colloid Interface Sci.*, Vol. 55, pp. 35-44, 1981.

3) J. Gregory, "Fundamentals of Flocculation," *Critical Reviews in Environmental Control*, Vol. 19, Issue 3, 1989.

4) R. Hunter, "Applications of the Zeta Potential," *Zeta Potential in Colloid Science*, Academic Press, New York, 1981.

5) M. Elimelech, J. Gregory, X. Lia, and R. Williams, "Surface Interaction Potentials," *Particle Depostion and Aggregation Measurement Modeling & Simulation*, Butterworth Heinemann Publishers, Boston, 1995.

6) J. Gregory, "The Role of Colloid Interactions in Solid-Liquid Separation," *Wat. Sci. Tech.*, Vol. 27, No. 10, pp. 1-17, 1993.

7) R. M. Pashley and J. N. Israelachvili, "DLVO and Hydration Forces between Mica Surfaces in Mg^{2+}, Ca^{2+}, Sr^{2+} and Ba^{2+} chloride solutions," *J. Colloid Interface Sci.*, Vol. 97, pp. 446, 1984.

8) J. Gregory, "Fundamentals of Flocculation," *Critical Reviews in Environmental Control*, Vol. 19, Issue 3, 1989.

9) R. M. Pashley and J. N. Israelachvili, "Measurement of the Hydrophobic Interaction between Two Hydrophobic surfaces in Aqueous Electrolyte Solutions," *J. Colloid Interface Sci.*, Vol. 98, pp. 500, 1984.

10) P. M. Claesson and H. K. Christenson, "Very Long Range attraction between Uncharged Hydrocarbon and Fluorocarbon Surfaces in Water," *J. Phys. Chem.*, Vol. 92, pp. 1650, 1988.

11) P. C. Hiemenz, "Principles of Colloid and Surface Chemistry, Second Edition," Marcel DekkerInc., New York and Basel, 1986.

12) J. Gregory, "Fundamentals of Flocculation," *Critical Reviews in Environmental Control*, Vol. 19, Issue 3, 1989.

13) E. Tipping, "Colloids in the Aquatic Environment," *Chem. Ind. (London)*, Vol. 15, pp. 485, 1988.

14) M. R. Jekel, "The Stabilization of Dispersded Mineral Particles by Adsorption of Humic Substances," *Water Res.*, Vol. 20, pp. 1543, 1986.

15) J. Gregory, "The Role of Colloid Interactions in Solid-Liquid Separation," *Wat. Sci. Tech.*, Vol. 27, No. 10, pp. 1-17, 1993.

16) J. Gregory, "Rates of flocculation of Latex Particles by Cationic Polymers, " *J. colloid Interface Sci.*, Vol. 42, pp. 448-456, 1973.

17) B. V. Deryagin and L. D. Landau, "Theory of the Stability of Strongly Charged Lyophobic Sols and of the Adhesion of Strongly Charged particles in Solutions of Electrolytes," *Acta Physicochim. URSS*, Vol. 14, pp. 733-762, 1941.

18) E. J. W. Verwey and J. Th. G. Overbeek, "Theory of the Stability of Lyophobic Colloids," Amsterdam: Elsevier, 1948.

19) J. Gregory, "Fundamentals of Flocculation," *Critical Reviews in Environmental Control*, Vol. 19, Issue 3, 1989.

20) T. Serra, and X. Casamitjana, "Modelling the Aggregation and Break-up of Fractal Aggregates in a Shear Flow," *Applied Scientific Research*, Vol. 59, pp. 255-268, 1998.

21) C. R. O'Melia, "Coagulation in Water and Wastewater Treatment," *Water Quality Improvement by Physical and Chemical Processes*, University of Texas Press, Austin and London, pp. 219-235, 1970.

22) C. R. O'Melia, and C. L. Tiller, "Physicochemical Aggregation and Deposition in Aquatic Environments," *Environmental Particles*, Lewis Publishers, New York, 1993.

23) M. R. Wiesner, "Kinetics of Aggregate Formation in Rapid Mix," *Wat. Res.*, Vol. 26, No. 3, pp. 379-387, 1992.

24) H. Han and D. F. Lawler, "Interactions of two Settling Spheres: Settling Rates and Collision Efficiency," *J. Hydraul. Eng.*, Vol. 117, pp. 1269-1289, 1991.

25) H. Han and D. F. Lawler, "The (Relative) Insignificance if G in Flocculation," *J. Am. Water Works Assoc.*, Vol. 84, pp. 461-474, 1981.

26) C. R. O'Melia, and C. L. Tiller, "Physicochemical Aggregation and Deposition in Aquatic Environments," *Environmental Particles*, Lewis Publishers, New York, 1993.

27) P. R. Hutchison, and T. W. Healy, "Coagulation and Flocculation - Destabilizing Practices? (with Particular Reference to Metal Ion Coagulants)," *Surface and Colloid Chemistry in Natural Waters and Water Treatment*, Plenum Press, New York, 1990.

28) I. Licsko', "Realistic Coagulation Mechnisms in the Use of Aluminium and Iron(III) Salts," *Wat. Sci. Tech.*, Vol. 36, No. 4, pp.103-110, 1997.

29) S. Farooq and S. G. Velioglu, "Physico-chemical Treatment of Domestic Wastewater," *Encyclopedia of Environmental Control Technology, Volume 3: Wastewater Treatment Technology*, Gulf Publishing Company, pp. 29-53, 1989.

30) J. Gregory, "Fundamentals of Flocculation," *Critical Reviews in Environmental Control*, Vol. 19, Issue 3, 1989.

31) F. de Dianous, E. Pujol, and J. C. Druoton, "Industrial Application of Weighted Flocculation: Development of the Actiflo® Clarification Process," *Chemical Water and Wastewater Treatment: Proceedings of the 4th Gothenburg Symposium 1990*, Madrid, Spain, October 1-3, 1990.

32) C. Cailleaux, E. Pujol, F. de Dianous, and J. C. Druoton, "Study of Weighted Flocculation in View of a New Type of Clarifier," *J. Water SRT-Aqua*, Vol. 41, No. 1, pp. 18-27, 1992.

33) Y. Ding, R. Dresnack, and P. Chan, "A Study of High-Rate Settling Process Kinetics: Microcarrier Weighted Flocculation-Clarification,"*Rep. EPA-7C-R364-NAFX*, USEPA, Cincinnati, Ohio, 1999.

34) R. Field, and T. P. O'Conner, "Optimization of CSO Storage and Treatment Systems," *J. Environ. Eng.*, Vol. 123, No. 3, pp. 269, 1997.

35) R. Field, T. P. O' Conner, R. Pitt, C. Y. Fan, S. Clark, J. Ludwig, and T. Hendrix, "Urban Wet-Weather Flows,"*Wet-Weather Flow Research Program*, National Risk Management Research Laboratory-Cincinnati, Edison, New Jersey, 1998.

36) V. Plum, C. P. Dahl, L. Bensten, C. R. Petersen, L. Napstjert, and N. B. Thomsen, "The Actiflo Method," *Proc. 2nd Int. Conf. The Sewer as a Physical, Chemical and Biological Reactor.*, Aalborg, Denmark, 1997.

37) E. Guibelin., F. Delsalle, and P. Binot, "The Actiflo® Process: A Highly Compact and Efficient Process to Prevent Water Pollution by Stormwater Flows," *Wat. Sci. Tech.*, Vol. 30, No. 1, pp. 87-96, 1994.

38) F. de Dianous and J. C. Dernaucourt, "Advantages of weighted Flocculation in Water Treatment," *Water Supply*, Vol. 9, pp. S43-S46, 1991.

39) B. B. Mandelbrot, "The Fractal Geometry of Nature," W. H. Freeman and Company, San Francisco, 1977.

40) S. J. Jung, R. Amal, and J. A. Raper, "Monitoring Effects of Shearing on Floc Structure Using Small-Angle Light Scattering," *Powder Technology*, Vol. 88, pp. 51-54, 1996.

41) P. Meakin, "Fractal Aggregates," *Adv. in Colloid and Interface Sci.*, Vol. 28, pp. 249-331, 1988.

42) R. Jullien and R. Botet, "Aggregation and Fractal Aggregates," World Scientific Publishing Co Pte Ltd., Singapore, 1987.

43) J. Gregory, "The Role of Floc Density in Solid-Liquid Separation," *Filtration & Separation*, Vol. 35, No. 4, pp. 367-371, May 01 1998.

44) M. R. Wiesner, "Kinetics of Aggregate Formation in Rapid Mix," *Wat. Res.*, Vol. 26, No. 3, pp. 379-387, 1992.

45) P. Meakin, B. Donn, and G W. Mulholland, "Collisions between Point Masses and Fractal Aggregates," *Langmuir*, Vol. 5, pp. 510-518, 1989.

46) D. H. Li, and J. Ganczarczyk, "Fractal Geometry of Particle Aggregates Generated in Water and Wastewater Treatment Processes," *Environ. Sci. Technol.*, Vol. 23, pp. 1385-1389, 1989.

47) F. Zartarian, C. Mustin, G. Villemin, T. Ait-Ettager, A. Thill, J. Y. Bottero, J. L. Mallet, and D. Snidaro, "Three-Dimension Modeling of an Activated Sludge Floc," *Langmuir*, Vol. 13, pp. 35-40, 1997.

48) S. J. Jung, R. Amal, and J. A. Raper, "Monitoring Effects of Shearing on Floc Structure Using Small-Angle Light Scattering," *Powder Technology*, Vol. 88, pp. 51-54, 1996.

49) P. T. Spicer, S. E. Pratsinis, J. Raper, R. Amal, G. Bushell, and G. Meesters, "Effect of Shear Schedule on Particle Size, Density, and Structure During Flocculation in Stirred Tanks," *Powder Technology*, Vol. 97, pp. 26-34, 1998.

50) T. D. Waite, "Measurement and Implications of Floc Structure in Water and Wastewater Treatment," *Colloids and Surfaces A: Physicochemical and Engineering Aspects*, Vol. 151, pp. 27-41, 1999.

51) J. Y. Bottero, D. Tchoubar, M. A. V. Axelos, P. Quienne, and F. Fiessinger, "Flocculation of Silica Colloids with Hydroxy Aluminum Polycations. Relation between Floc Structure and Aggregation Mechanisms," *Langmuir*, Vol. 6, pp. 596-602, 1990.

52) J. Zhang and J. Buffle, "Multi-Method Determination of the Fractal Dimension of Hematite Aggregates," *Colloids and Surfaces A: Physicochemical and Engineering Aspects*, Vol. 107, pp. 175-187, 1996.

53) S. B. Grant, C. Poor, and S. Relle, "Scaling Theory and Solutions for the Steady-State Coagulation and Settling of Fractal Aggregates in Aquatic Systems," *Colloids and Surfaces A: Physicochemical and Engineering Aspects*, Vol. 107, pp. 155-174, 1996.

54) S. R. Forrest and T. A. Witten, "Long-Range Correlations in Smoke-Particle Aggregates," *J. Phys A: Math. Gen.*, Vol 12, pp. L109-L117, 1979.

55) M. Tence, J. P. Chevalier, and R. Jullien, "On the Measurement of the Fractal Dimension of Aggregated Particles by Electron Microscopy: Experimental Method, Corrections and Comparison with Numerical Models," *J. Physique*, Vol. 47, pp. 1989-1998, 1986.

56) L. G. B. Bremer, B. H. Bijsterbosch, P. Waistra, and T. van Vilet, "Formation, Properties, and Fractal Structure of Particle Gels," *Adv. in Colloid and Interface Sci.*, Vol. 46, pp. 117-128, 1993.

57) A. C. Pierre, K. Ma, and C. Barker, "Structure of Kaolinite Flocs Formed in an Aqueous Medium," *J. of Material Sci.*, Vol 30, pp. 2176-2181, 1995.

58) J. Zhang and J. Buffle, "Multi-Method Determination of the Fractal Dimension of Hematite Aggregates," *Colloids and Surfaces A: Physicochemical and Engineering Aspects*, Vol. 107, pp. 175-187, 1996.

59) A. Cornelissen, M. G. Burnett, R. D. McCall, and D. T. Goddard, "The Structure of Hydrous Flocs Prepared by Batch and Continuous Flow Water Treatment Systems and Obtained by Optical, Electron and Atomic Force Microscopy," *Wat. Sci. Tech.*, Vol. 36, No. 4, pp. 41-48, 1997.

60) D. Snidaro, F. Zartarian, F. Jorand, J. Y. Bottero, J. C. Block, and J. Manem, "Characterization of Activated Sludge Flocs Structure," *Wat. Sci. Tech.*, Vol. 36, No. 4, pp. 313-320, 1997.

61) W. Liang, and K. Kendall, "Aggregate formation in Colloidal Dispersions," *Colloids and Surfaces A: Physicochemical and Engineering Aspects*, Vol. 131, pp. 193-201, 1998.

62) Standard Methods for the Examination of Ware and Wastewater, 7th Edition, Edited by Lenore S. Clesceri, Arnold E. Greenberg, and R. Rhodes Trussel, Prepared and Published by American Public Health Association, American Water Works Association and Water Pollution Control Federation, 1989.

63) The ElectroScan Operator's Manual, The Environmental Scanning Electron Microscope Model 2020, ElectroScan Corporation, Wilmington, Massachusette, 1994.